PRACTICAL EXPERIMENTS AND SIMULATIONS FOR NUCLEAR SAFEGUARDS EDUCATION

A Thesis
presented to
the Faculty of the Graduate School
at the University of Missouri-Columbia

In Partial Fulfillment
of the Requirements for the Degree

Master of Science

by
JOHN BALL

Dr. John Gahl, Thesis Supervisor

MAY 2007

The undersigned, appointed by the dean of the Graduate School, have examined the thesis entitled

PRACTICAL EXPERIMENTS AND SIMULATIONS FOR NUCLEAR SAFEGUARDS EDUCATION

presented by John Ball,

a candidate for the degree of master of electrical engineering,

and hereby certify that, in their opinion, it is worthy of acceptance.

Professor John Gahl

Professor Kathleen Trauth

Professor Naz Islam

ACKNOWLEDGEMENTS

I would like to thank Dr. John Gahl and Dr. Kathleen Trauth for all of their help in preparing, executing, and presenting all parts of this research. All of the engineering students that took part in the Nuclear Safeguards course as well as the staff of the University of Missouri Research Reactor deserve thanks for their part in allowing this research to reach completion. In addition, the prior work in this area by Josh Neustrom helped greatly toward the amount of progress that was made in the new nuclear safeguards science and technology program at the University of Missouri.

TABLE OF CONTENTS

LIST OF ILLUSTRATIONS

LIST OF TABLES

Chapter 1 Introduction

Recently the University of Missouri-Columbia has implemented a Nuclear Safeguards graduate certificate to help satisfy the need for increased accountability in the growing field of nuclear technology. In order to fulfill partially the requirements of this certificate, a Nuclear Safeguards Science and Technology course has been established to link the concepts of nuclear science with those of nuclear security. Courses have already been available to allow a student to become familiar with the nature and properties of radioactive isotopes as well as their nonproliferation risks and other associated hazards. However, this new course strives to provide access to the methods and principles that connect the concepts of nuclear science with their applications to the safeguarding of nuclear materials.

In recent years, the need for nuclear safeguards has risen with the increasing interest in nuclear power and the rising threat of nuclear weapons. Currently, many professionals in nuclear safeguards are reaching the age of retirement, creating a need for new talent in the field. Because these professionals have often been trained primarily as the path of their careers required, few possibilities for nuclear safeguards education have been established to encourage and train future safeguards professionals. Specifically, few laboratory exercises or other hands-on activities have been designed for this training. It is the purpose of this thesis to help rectify this issue by providing tools and example experiments to aid in future safeguards education.

The three primary aspects of nuclear safeguards are material protection, control, and accountability. First, a tool is developed using a statistical model called EASI that can be used to aid in the design of physical protection systems. Secondly, an example

laboratory experiment is presented that shows a calibration of a hand-held radiation detector for the use in preventing theft of a radioisotope for the purpose of material control. Finally, the development of a script in MATLAB for use in simulating gamma ray spectra, a method commonly used in material accounting, for various radioactive isotopes is presented.

Chapter 2 Background

Physical Protection

While material control and accounting are primarily used to detect a diversion or theft of material from an inside source through careful attention to existing inventories of nuclear material, another aspect of materials protection, control, and accountability (MPC&A) consists of protecting nuclear material from an external threat. This area, usually known as the physical protection of a specified target, involves the detection of an intruder, the delay of the intruder's progress, and the response of a guard team in order to intercept the intruder. Regarding nuclear safeguards, the targets to be protected can usually be considered to be stored nuclear material, though schematics, records, and other information can be considered potential targets for intruders. In addition, an adversary's intent is not limited to theft, but could also be a form of sabotage, through both direct or indirect means, such as instilling doubt on nuclear security in general. For the sake of modeling protection systems, all targets discussed here are treated equally.

Ideally, in order for a physical protection system to accomplish its goal effectively, an intruder must be detected as quickly as is reliably possible, and barriers need to deter the intruder for as long as necessary to allow a guard force to respond. For instance, a motion sensor placed at the entrance to the road leading to a facility might detect all intruders, but it would also be likely to detect a large portion of movement that would be completely unrelated to the facility in question. On the other hand, signals from a motion sensor placed directly by the target to be protected would be very reliable, but any information about an intruder would not arrive quickly enough to allow a guard force to

respond. For this reason, a suitable balance is necessary between detection and delay. In addition, delay is unnecessary if there is no detection at the location in question.

Due to the inherently unpredictable nature of systems involving interaction between humans and machines, a certain level of abstraction is necessary to mathematically predict the outcome of most situations. Typically, statistical models are used to approximate the relative effectiveness of one system configuration with regard to another. These models typically do not represent an accurate description of a real invasion to a facility, but rather predict what each component will contribute to the overall effectiveness of the system. Each factor in the physical protection system can change the probability that an adversary will accomplish his or her goal. Some of these factors are well-defined and can be modified by effective design, while other factors are less clear-cut and require a more intimate knowledge of the facility as well as potential threats [1].

Factors That Affect a Physical Protection System

Detection

Any component in the system that can signal that an adversary has invaded the facility to be protected has a certain reliability that can be approximated by using a percentage, which is known as its probability of detection. This reliability can vary greatly depending on different conditions, such as weather or the movement pattern of an adversary. As would be expected, most sensors exhibit more predictable behavior under controlled conditions. This presents a design conflict, as outdoor sensors are more desirable from a statistical standpoint, but can also be less reliable due to varying conditions. Numerical probabilities of detection are inherently inaccurate, and are

usually interpretations of approximate descriptions of a sensor's reliability under certain conditions. For instance, a passive infrared motion sensor placed indoors in a dimly lit environment might be described as "good," and assigned a probability of detection of 90%. On the other hand, this same detector, when placed outdoors in a humid environment might only be described as "fair" at night and "bad" during the day. Under these conditions, this sensor might be given approximate probabilities of detection of 70% and 50%, respectively. In this manner, exact predictions of the effectiveness of a detector are nearly impossible, but these approximate percentages can help reveal information about the locations of potential weaknesses in an overall system. Useful information can be collected about sensors on a trial and error basis, in which detectors are tested many times. In a report by Sandia National Laboratories [2], several standard detectors have been investigated under varying conditions, and their relative reliabilities recorded. In some cases, however, the effectiveness of a sensor is loosely based on anecdotal evidence, and further testing is necessary.

Delay

While detection is critical in alerting a guard force that a response is necessary, the element of delay in a physical protection system provides the guard force with the ability to effectively deal with the threat. Fundamentally, most barriers for delay consist of strong doors and locks, though other, more innovative barriers have been devised. Outer barriers, such as fences with barbed wire, are usually not considered a form of delay, as detection often does not occur at this level of the protection system. Rather, outermost barriers are considered a form of deterrent. Since deterrence is virtually impossible to account for, it is ignored when analyzing the effectiveness of a physical

protection system. Elements of delay can be located at many points in a system, but are the most effective when placed such that they slow an adversary at locations that facilitate their interruption by a guard force. This can mean that the adversary is easily detected, easily detained, or a combination thereof. In practice, effective barriers with longer delays are typically placed closer to the target to be protected. Barriers and detectors depend upon one another to maximize the effectiveness of the overall system.

Response

Once an adversary in a facility has been detected, it is the responsibility of the response force to arrive and interrupt the adversary. The means with which this guard force accomplishes this task depends on the scenario. The success of the response force depends on many complex factors such as timing, training, and number. Experimental evidence has shown a correlation between the success of the guard force and the relative sizes of the guard force versus the adversaries. However, for some simpler statistical models, the success of the response team is assumed to be related only to the reliability of the alarm communication system and the average response time.

Material Control

While physical protection systems are designed to keep intruders from infiltrating a facility and stealing or otherwise causing damage to its assets, material control and accounting work together to prevent malicious actions from within the facility. Material control, specifically, refers to the element of nuclear safeguards that ensures the integrity of every part of the nuclear facility as a whole. This subject encompasses many aspects of safeguards, from investigating new employees to keeping track of special nuclear material (SNM) movements within the facility [3]. A variety of equipment for material

control is available, from container seals that provide evidence if tampering has taken place to passive monitoring systems that are able to track the movement of items or bulk material within a section of a facility. However, much of material control exists in policy form, such as the security screenings that new employees are subjected to and the policy that two people are to oversee movements of SNM within a facility, called the "two-man" rule.

On the organizational level, material control is overseen in terms of domestic and international safeguards. On the domestic level, safeguards and material control specifically are handled by the United States Department of Energy and the Nuclear Regulatory Commission. Regulations concerning material handling, shipping, and security are found in Title 10 of the Code of Federal Regulations. Typically, domestic safeguards deal with the possibility of individuals or independent organizations misusing nuclear material. International safeguards are handled by the International Atomic Energy Agency (IAEA). The IAEA is the United Nations (UN) body that deals with the global community as a whole by advising the UN regarding the nuclear activities and aspirations of individual nations [3].

Material Accounting

An important aspect of material accounting is the ability to verify that the amount and isotopic composition of SNM in a sample is accurately known. Regarding nuclear safeguards, this is important for intermittent inventories of nuclear material, the determination of the isotopic composition of fuel elements before or after their use, and the investigation of unknown materials. In many cases, it is simply important to verify theoretical calculations with actual measurements. In other cases, such as the flow

processes in enrichment facilities, the isotopic composition of hold-up material in the flow systems can be significant not just for SNM regulation, but also for the proper operation of the equipment.

For nuclear material accounting, the various methods used can typically be classified as belonging to one of two categories: nondestructive analysis (NDA) or chemical assay. Nondestructive analysis involves the assessment of properties inherent to the subject material, such as mass or radioactive emissions. Chemical assay, however, usually involves processes that cause a chemical or physical change in the subject material such as dilution, dissolution, or ignition. The sample material that is measured by chemical assay is often destroyed or simply discarded. NDA methods can be further categorized as active or passive methods. Passive methods often involve the measurement of pre-existing properties of the material, while active methods require some sort of activation (such neutron-induced fission) for a measurement.

Many passive NDA methods involve the measurement of radiation that has either originated from or interacted with the sample to be analyzed. Of these methods, many deal specifically with gamma radiation. Typically, the gamma ray spectrum emitted by a sample is detected with an appropriate sensor and then analyzed by a multi-channel analyzer. The sensor "picks up" gamma rays that interact with the sensor material, creating charge separations that can be detected. In the case of Geiger-Müller based detectors, the detection gas is ionized by incident radiation, and the resulting free electrons are collected by a positively charged probe, where they are detected as current. Scintillation detectors sense radiation by amplifying and detecting the light that results from the fluorescence of radiation sensitive material. In the case of solid-state detectors,

incident gamma rays create electron-hole pairs in the semiconductor crystal, and this pair is swept away as current by an applied voltage. Since the mean free path of gamma rays in solids is typically much lower than that for gases or liquids, solid-state detectors have been found to be much more efficient for gamma ray spectroscopy.

Depending on the scale and homogeneity of the sample, certain methods can also be used that determine the composition of the material by analyzing the attenuation of externally emitted radiation through a cross-section of the sample.

Chapter 3 Material Protection

The Development and Application of a Tool for Physical Protection System Design Using EASI

Many analytical tools have been developed to aid in the design of physical protection systems. The basis for this analysis is the "Estimate of Adversary Sequence Interruption" (EASI) system that is organized as a computer spreadsheet [1]. A sample EASI spreadsheet can be found in Appendix A. Through numerical analysis of EASI, a tool has been developed that can augment its use in the improvement of existing system designs as well as helping to understand the fundamental principles of protection system design [4]. With this tool, judgments can be made regarding the effectiveness of the individual components of a system, and the ideal locations for additional components can be determined. Furthermore, cost analyses can be quickly and efficiently performed by determining the effectiveness of various detectors when implemented alone or in coordinated groups.

When given the physical protection system for a facility with known performance parameters, one can insert these parameters into an EASI spreadsheet and receive a statistical estimate for the effectiveness of the system. This estimate is in the form of the probability that an adversary's sequence to a desired target will be successfully interrupted by a response force. When using EASI, it is necessary to have approximate detection probabilities for the implemented detectors as well as estimates for the amount of delay that the protection system presents to an adversary. When designing a protection system, it is desirable to be able to determine what can be done to improve the overall

system rather than simply observing how adjustments to the system change its performance.

Introduction of Relevant Terms

For the purpose of clarity, it is necessary to define some terms that are specific to this kind of analysis of a physical protection system (PPS). For this statistical approach, the amount of delay between a sensor and the target area to be protected (D) is more useful than the physical location of the detector. For this reason, the locations of sensors will be given as amounts of delay that will be referred to as their "delay locations." The total amount of delay (TD) that a PPS presents to an adversary needs to be known; as does the amount of time it takes a response force to arrive (RFT). Generally speaking, most of this analysis is performed with regard to the ratio of the response force time to the total delay, which will be called the response time ratio (RR), where RR=RFT/TD. The ratio of D to TD for the PPS is called the delay ratio (DR), where DR = D/TD. The reliability of a sensor is referred to as its probability of detection (P_D), and the overall effectiveness of a PPS is called its probability of interruption (P_I).

Assigning Probabilities of Detection to Sensors

For detectors used in physical protection systems, the probabilities of detection vary due to many factors beyond the control of the system designer. For this statistical analysis, approximate average values are used. These probabilities can be found in Sandia National Laboratories' report SAND91-0948 [2] and are labeled with the qualitative probabilities of "very low," "low," "medium," "high," and "very high." For the sake of this analysis, probabilities of 10%, 25%, 50%, 75%, and 90%, respectively, are assigned to these labels. These values are used by Garcia in the text *The Design and*

Evaluation of Physical Protection Systems [1]. Mathematically speaking, a margin of error in the P_D value for a sensor will produce no more than that same margin of error in the system's P_I.

Assumptions also need to be made with regard to the amounts of time used for delays and for the response force. For the sake of EASI analysis, standard deviations are assumed to be approximately one-third of the average values used. Assuming that the average values used for delays and the RFT are valid, this approach will include most of the "worst-case scenario" values, such as near-zero delay times and response force times that are twice the stated average value.

Analysis

Figure 1 shows the relationship between a sensor's contribution to the P_I of a PPS as a function of its given P_D value. The individual lines show the effect that the sensor's delay location has on P_I. The graph shows that the relationship is linear and also that a sensor's contribution to P_I increases for increasing DR values. The lines of increasing slopes indicate this phenomenon. As the DR value for a sensor located in a PPS increases, its maximum possible contribution to P_I increases as well. This pattern of lines suggests that the detector's contribution to P_I is a function of its DR value and is scaled by the actual P_D value of the sensor. A plot of P_I versus D for an ideal detector (Figure 2) shows what one would expect: the further a detector lies from the intended target (in "delay seconds") the more it contributes to P_I. On the other hand, a detector placed near the target it is meant to protect contributes very little to P_I. Given the linear relationship between P_I and P_D, this graph can be used for detectors of any reliability. In that case, the corresponding P_I value is simply multiplied by the sensor's P_D value. This technique

makes an assumption that the amount of delay present in the system before the first detector encountered by an adversary is either very small or is not taken into account.

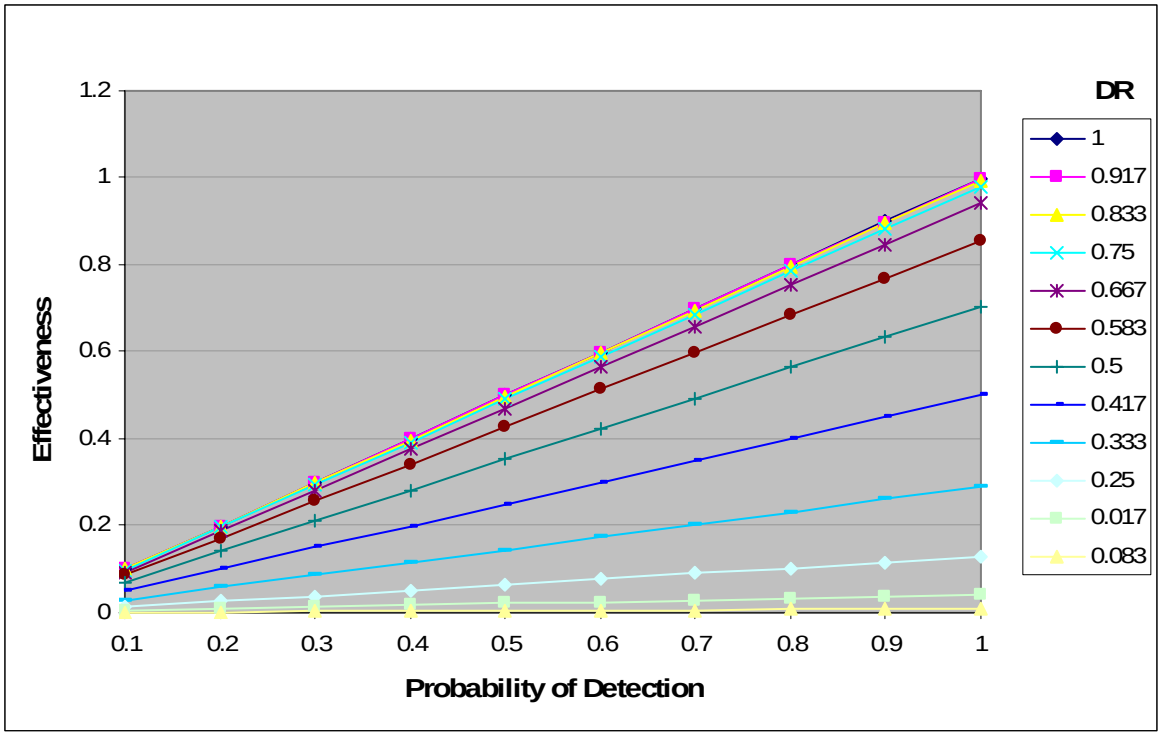

Figure 1 Effectiveness of a Detector as a Function of its Probability of Detection.

It is apparent, however, that if the RFT is too large, the P_I will be lower. To account for this, the detector curve is reproduced for varying response times. The graph (Figure 3) shows the different curves that arise for RR values between between 0 and 1. As one would expect, a near-zero response time ratio corresponds to a graph that is nearly constant at a value of 1, whereas the maximum P_I for RR=1 is 50%. This observation is intuitive, as a response force that arrives in an amount of time equal to the total delay in the system will be able to interrupt only the half of adversaries that take longer than the average amount of time to infiltrate the PPS.

This family of curves can be used to determine the effect a sensor at a given delay location will have on the P_I of a PPS with a certain RR value. The sensor's contribution to P_I lies on the y axis, and DR lies on the x axis. For instance, if a detector has a delay location of 200 seconds, TD is 400 seconds, and RFT is 300 seconds, then the value of the RR = .75 curve at DR=.5 will give that detector's contribution to P_I.

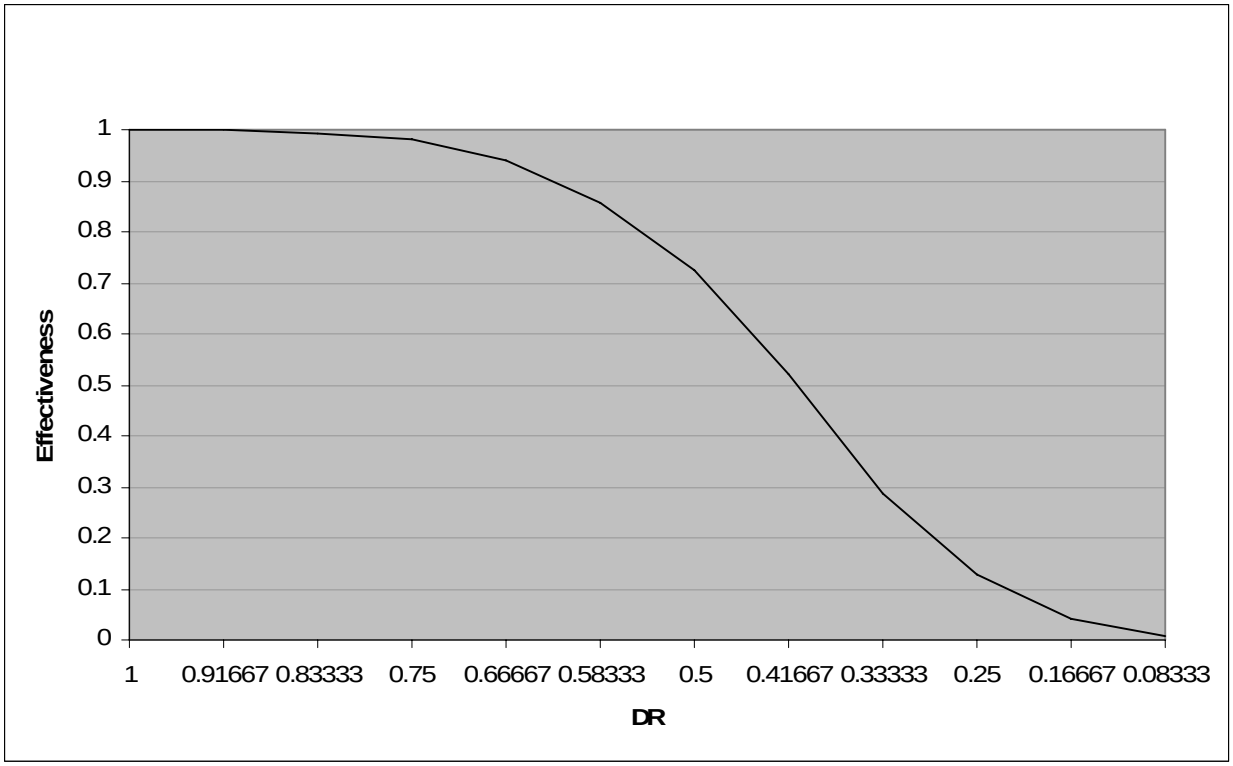

Figure 1 Effectiveness of an Ideal Detector as a Function of its Delay Location.

Most protection systems implement more than one sensor. The contributions of subsequent detectors are found by adding the P_I of each detector for proportion of adversaries that the previous sensors do not detect. For example, if three detectors exist in a system at different points with probabilities of detection P_1, P_2, and P_3, P_I is approximated by equation 1, where P_{Gi} is the percentage found from the graph for detector i and P_C is the probability of successful guard communication;

$$P_I = P_C(P_1P_{G1} + (1-P_1)P_2P_{G2} + (1-P_1)(1-P_2)P_3P_{G3}). \quad (1)$$

Given this family of curves, it is simple to not only judge the effectiveness of a certain detector when given P_D, D, and RFT, but also to estimate the optimum location for a detector to achieve a desired probability of interruption. For instance, if the RR for a system is 0.5, and the desired contribution of a sensor is 75%, then the appropriate delay location would be approximately 60% or more of its TD. It is easy to predict, using the graph, how this result would change if other parameters for the system were to change.

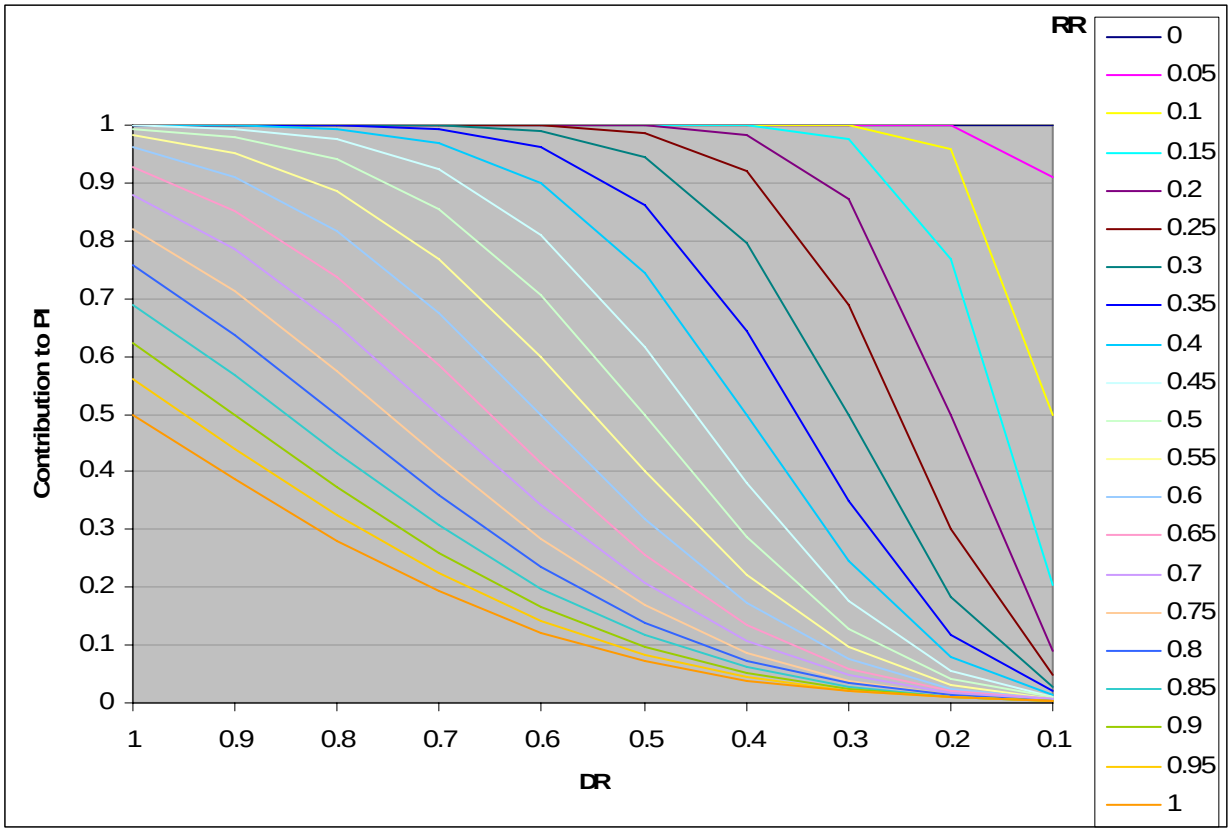

Figure 3 Contribution to P_I of a Detector as a Function of its Delay Location.

When examining the family of curves that arises from this analysis, some characteristics of the mathematical and statistical workings of this EASI spreadsheet become evident. As noted earlier, if the delay location of any one sensor is equal to the guard response time, the maximum contribution of that sensor is half of its probability of detection. Indeed, the contribution by any sensor at a DR value equal to the system's RR value is exactly half of its P_D value (Figure 4). This phenomenon is a result of the underlying statistical methods used. In other words, one would expect the response force to be able to interrupt the proportion of intruders that would take longer than the average response time to achieve its goal—namely, half.

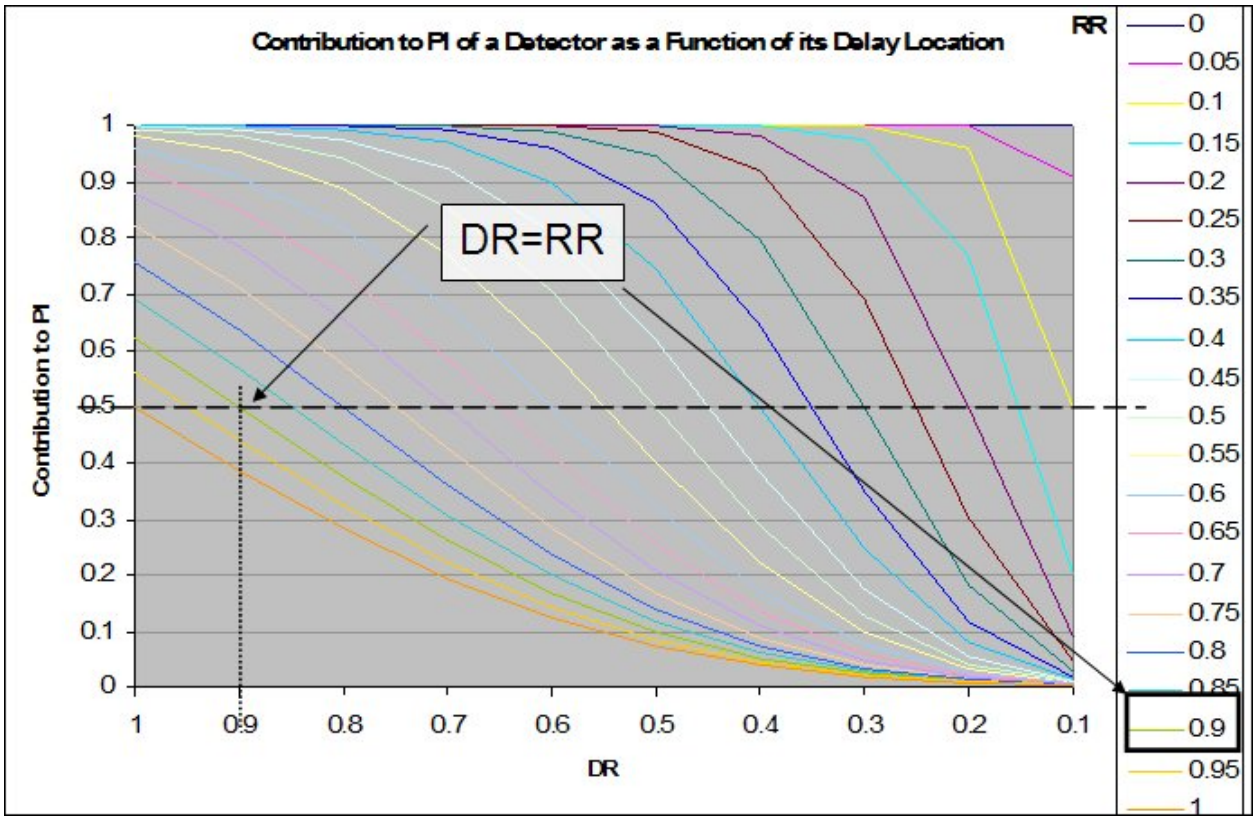

Figure 4 Contribution Relationship when RR = DR.

Applicable Scenarios

In the following section, some scenarios are presented that exhibit how one would use the conclusions and tools developed here to enhance existing physical protection systems. The examples given are not complex, but this simplicity does not invalidate the usefulness of this analysis.

Scenario 1

A physical protection system designer would like to improve the security of the facility shown in Figure 5 that has the characteristics provided in Table 1 as well as a 95% probability of successful guard communication. An initial EASI analysis shows that the average probability of interruption for the system is 84.4% in its current state. When looking at the family of curves for this system in Figure 6 with the proper RR curve emphasized as shown, it can be seen that all existing sensors (marked with dots) are placed such that their DR value does not cause a large decrease in their maximum contribution to P_I. Seeing this, the designer opts to concentrate on improving the effectiveness of the individual sensors rather than on maximizing delays.

Figure 7 and Table 2 show the decisions made by the designer. The response ratio has improved slightly due to a combination of placing stronger locks on the doors and improving the response force time. Additionally, the two sensors have been replaced to provide a greater probability of detection. Analyzing these improvements in the EASI spreadsheet yields a new average probability of interruption of 92.3%. Note that even though the possible contribution by a third sensor placed at the inner building has increased significantly, the additional contribution by a sensor at this point is inherently

small due to its placement as the third sensor in the path. In this case, even an ideal sensor at this location would have a maximum contribution of 0.5% to the overall probability of interruption.

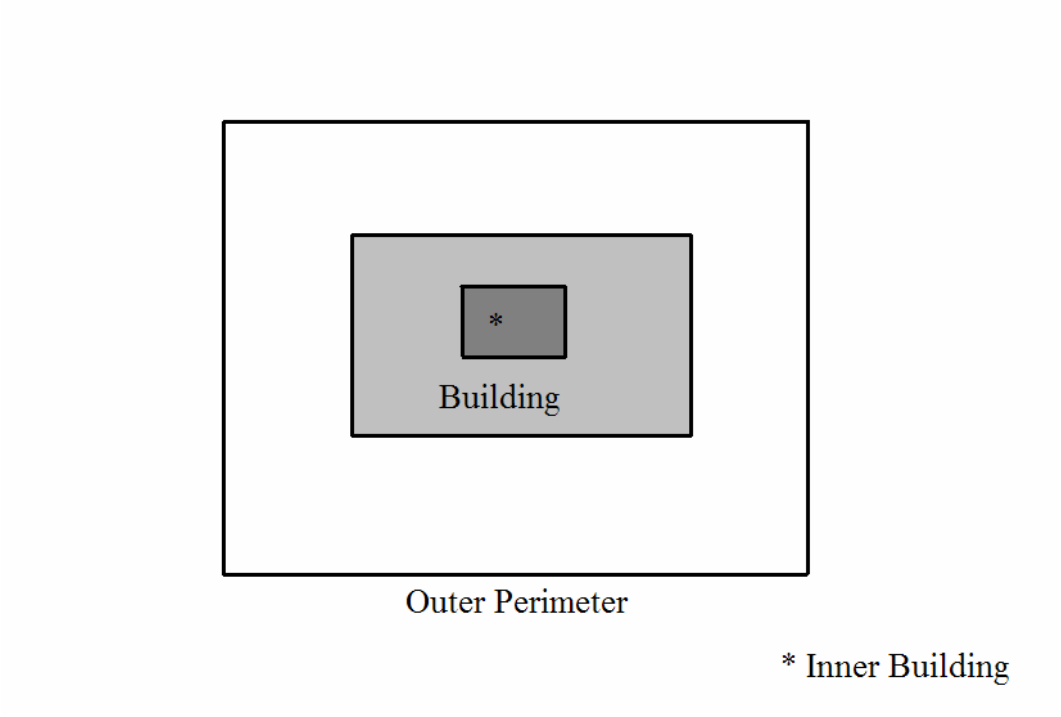

Figure 5 Simplified Fictitious Facility for Scenario 1.

Table 1: Original PPS Parameters for Scenario 1.

Location	P_D	Delay		RFT
Outer Perimeter	75%	.5 minutes		3 minutes
Outer Building	80%	3 minutes		
Inner Building	0%	2 minutes		

Scenario 2

A research reactor has a single path by which an intrusion could be attempted. The path delays consist of an outer fence, a locked front door, an inner door leading to the laboratory areas, and a pair of reinforced containment doors. An infrared motion sensor is mounted near the front door such that any attempt at forced entry will likely be

detected. Each containment door presents an estimated average of two minutes of delay, and the front door and inner door present one minute of delay each. It is expected that an adversary would need ten seconds, on average, to traverse the outer fence, and then another 30 seconds to reach the front door. The probability of the motion sensor detecting an adversary running or walking toward the sensor is considered "high," and so a value of 75% will be used for statistical purposes. A local guard force can respond within five minutes using a communication system that is 95% accurate. These parameters are listed in Table 3.

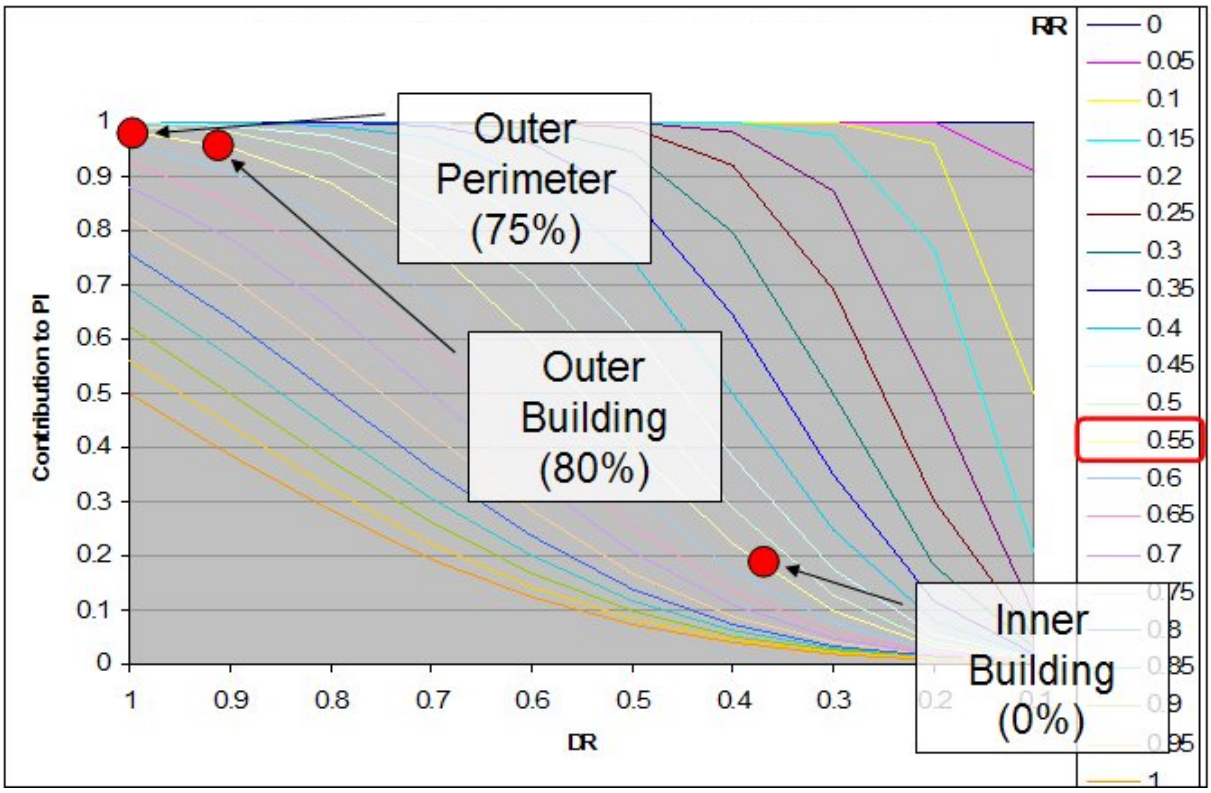

Figure 6 Original System Parameters for Scenario 1.

Table 2 Revised PPS Parameters for Scenario 1.

Location	P_D	Delay		RFT
Outer Perimeter	90%	.5 minutes		2.7 minutes
Outer Building	90%	3.5 minutes		
Inner Building	0%	2.5 minutes		

From an initial EASI analysis, it can be seen that the average probability of interruption for this scenario is 50.5%. Because the ratio of response force time to total delay time is approximately 0.75, the family of curves shows that the maximum probability of interruption that can be attained by any one sensor is ~82.5% of its probability of detection. In this case, the most rewarding change that could be made to the system is the reduction of the response force time. By lowering the RR ratio to 0.5 by either lowering the RFT to 200 seconds or raising the delay time to 600 seconds (or a combination thereof), the maximum contribution of a single sensor to P_I increases to ~98% of its P_D. In this case, P_I from a single PIR motion sensor at the front door increases to 66.2%. At this point, integrating a boundary detection system at the fence with a "high" probability of detection (such as a passive sonic detector) further increases P_I to 84.3%. It is worth noting that additional sensors added to the system will only contribute a significant amount to the probability of interruption if they lie more than 200 "delay seconds" away from the target that is to be protected.

Table 3: PPS Parameters for Scenario 2.

Location	P_D	Delay		RFT
Outer Perimeter	0%	0.15 minutes		5 minutes
Front Door	75%	1.5 minute		
Laboratory Door	0%	1 minute		
Containment 1	0%	2 minutes		
Containment 2	0%	2 minutes		

Scenario 3

A facility very similar to that of scenario 2 also has emergency exits that could be used to gain entry into the facility. These doors, which are protected by a motion detector similar to the one on the front door to the facility, lead directly to the laboratory area for safety reasons. These doors present, on average, a 60 second delay for an intruder trying

to pass through them, but allow the adversary to bypass the front door and the secondary lab door on the way to the target in the containment area.

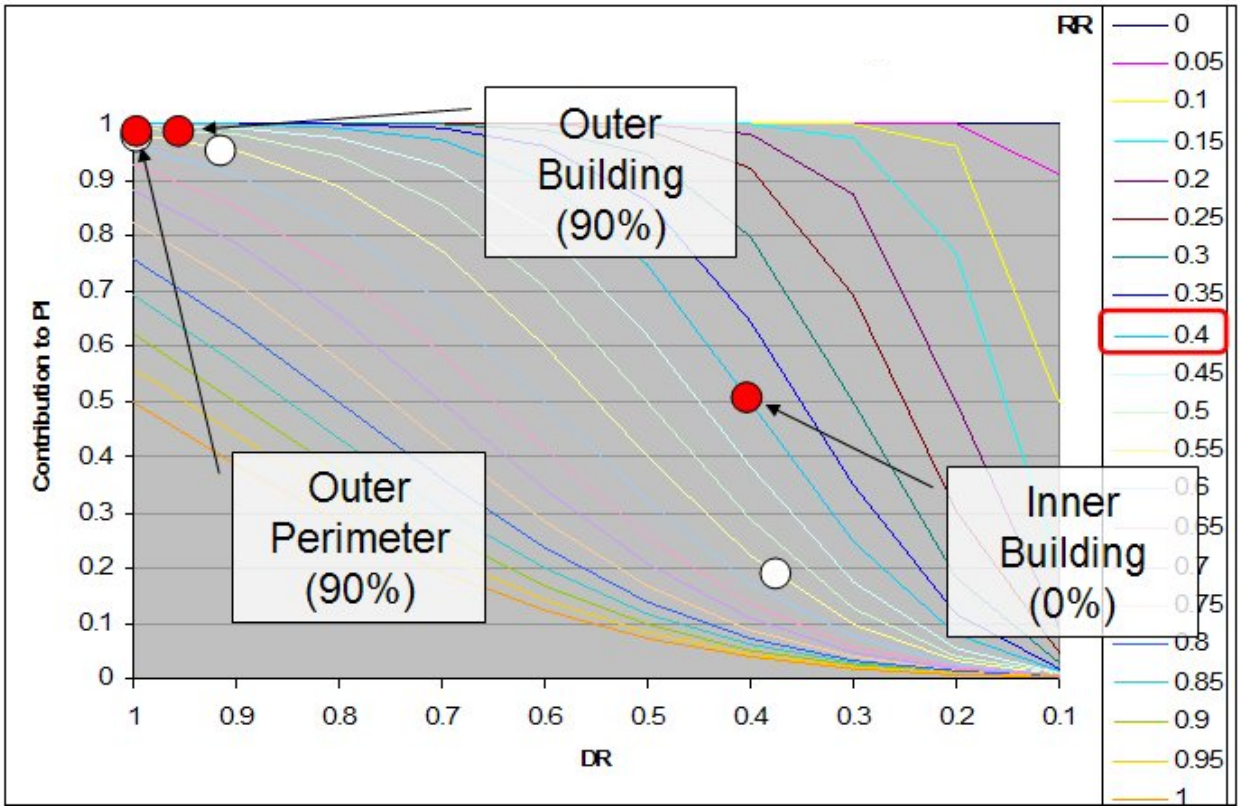

Figure 7 Comparison of Parameters for Scenario 1.

This presents two possible paths for an intruder. The path that leads through the front door still presents a P_I of 84.3%. The path through the emergency doors gives a P_I value of 76.2%. To balance the protection throughout the system, the path through the emergency doors needs to be improved. Assuming that the guard response time cannot be shortened; either the total delay or the detector's P_D should be improved.

For the most balanced protection throughout, the probability of detection at the emergency door should be improved, or the delay between the emergency door and the

containment doors should be increased. Improving the delay of the containment doors or the detection probability at the fence will improve the entire system's performance, which could be a desirable effect. In this case, other design considerations should be taken into account when choosing which aspects of a system to improve. By supplementing the motion sensor at the emergency door with a magnetic door switch, P_D at that location increases to 0.975, which increases the P_I for that path to 80.5%. If the motion detector is left alone and the delay time of the emergency door is doubled to 2 minutes (possibly using security bars or a rolling shutter), P_I becomes 84.3%. If the cumulative delay of the two containment doors was increased by one minute, rather than increasing the delay at the emergency door, the probability of interruption for the emergency door path would remain at 84.3%, but the front door path would then increase to 87.7%. By using the family of curves, it is easy to determine which parts of a protection system should be improved to obtain the largest increase in overall system performance.

Discussion

The manipulation of EASI applied here produces a tool that can be used to design or improve a physical protection system by identifying key points in the path of an adversary. From this analysis, it is clear that applying a statistical study to the EASI method yields some general results that can be used in the development or improvement of a physical protection system. As one would expect, a detector placed in a protection system at a point where the average response force time is equal to the average amount of delay will contribute 50% of its reliability to the probability that an intruder will be interrupted. Given the family of curves describing P_I versus DR, it can be seen that

detectors placed closer to the target than this point in the system will be much less effective, while detectors placed beforehand will be more effective. The ideal location for detectors in a protection system is at or after the point at which the remaining delay in the system is twice as long as the response force time. Reliable sensors are always desirable; however, a collection of less-reliable detectors can often be used in lieu of one highly-reliable detector with similar results. In any case, this approach might be more desirable due to other design constraints such as varying conditions at the facility's location. With all of these facts in mind, the method and tools shown here give a useful view of the design of protection systems that can have both practical and educational benefits.

Chapter 4 Material Control

Evaluation of the Canberra-Aquila Mini-Radiac as a Detection System in the Nuclear Safeguards Demonstration System at the University of Missouri Research Reactor

At the University of Missouri Research Reactor (MURR), a demonstration safeguards system has been installed for educational purposes. This Canberra Aquila surveillance system is very similar to those that have been set up successfully in various nuclear facilities in Russia by the Department of Energy's MPC&A Operational Monitoring (MOM) program. This system uses seven cameras to monitor various locations in the facility. These cameras utilize on-board microprocessors and motion sensing algorithms to detect and record motion according to parameters determined by the operator of the system. The pictures recorded are saved for future review, but could easily be monitored in real-time as well. In addition to periodic surveillance and motion-triggered events, each camera can be triggered by an external input that can be configured appropriately for the situation. Typical applications for this interface include magnetic door sensors and external motion detectors. A more comprehensive description of the system is published in the proceedings record of the 2004 INMM conference [5].

At MURR, one camera of the system is connected to a portable radiation detector called a Mini-Radiac. This detector, manufactured by Canberra, is a gamma ray detector designed for emergency response applications that is based on a Geiger-Muller tube. Previous experiments have shown that this detector can be configured to trigger a camera in the protection system by a radioactive source. The electronic circuitry that interfaces

between the detector and the system, as well as the mounting hardware for the detector, have been described earlier [6].

Evaluation of Detection Sensitivity

Using two small radiation sources, the response of the Mini-Radiac at various distances was examined. The first source was a 43.8 μCi Cesium-137 source, and the second, a 3.8 μCi Cobalt-60 source. The reading on the Mini-Radiac was recorded for distances between 1 cm and 150 cm from each source. It was found that the recorded radiation exposure fell off to the background level of 30 μR/hr within 150 cm of the radiation source. The readings are as shown in Figures 8 and 9. When registering the amount of gamma ray exposure, the Mini-Radiac took approximately 5 seconds to settle to the reading that was recorded. In the presence of a high level of exposure when compared to the background radiation, the Mini-Radiac would register a change almost immediately, and then oscillate as it settled to the actual value.

The readings given in Figures 8 and 9 were taken once the read-out had steadied. Usually, the read-out would immediately signal change, but the initial response was only marginally stable. For the sake of practicality, an exposure rate of 100 μR/hr was considered the lower limit for readings that could be easily distinguished from background noise. A smaller source such as the ones used here would need to pass relatively close to the Mini-Radiac in order to reliably register its presence. Using interpolation, the distance at which the detector would register 100 μR/hr from the Co-60 is 22 cm, compared with 74 cm for the Cs-137. It may prove difficult to place a Mini-Radiac in a doorway such that a source of this activity would surpass the 100 μR/hr threshold. Therefore, this system would be better suited for the detection of larger

activity sources. In a typical siting senario, the Mini-Radiac would likely be placed by a doorway, in a hallway, or on a ceiling. Assuming that the minimum exposure rate needed for accurate detection is 100 μR/hr and that the average maximum necessary distances for doors, hallways, and ceilings would be 120 cm, 240 cm, and 360 cm, respectively, the minimum amounts of activity needed for accurate detection can be calculated. These results are shown in Table 4. The amount of activity required for detection is proportional to the square of the distance.

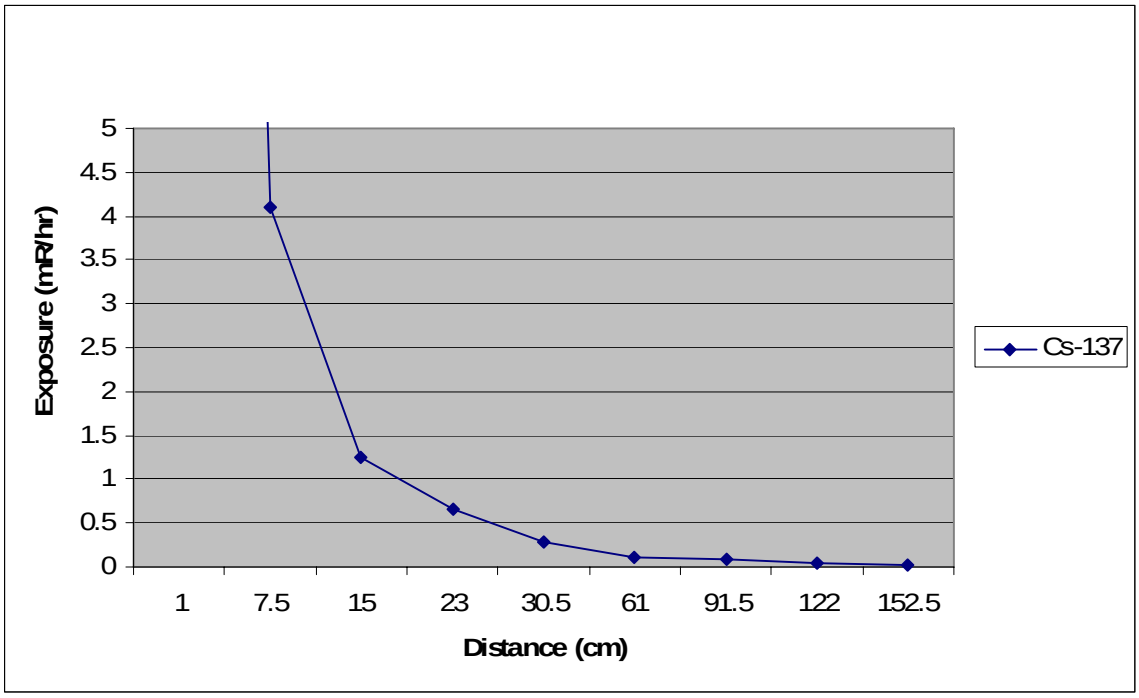

Figure 8 Exposure Rate Detected by Mini-Radiac from Cs-137 Source.

Table 4 Estimated Amount of Activity Required for Detection Utilizing Mini-Radiac.

Type	Distance	Co-60 Activity	Cs-137 Activity
Doorway	120 cm	115.2 μCi	480 μCi
Hallway	240 cm	460.8 μCi	1.92 mCi
Ceiling	360 cm	1.04 mCi	4.32 mCi

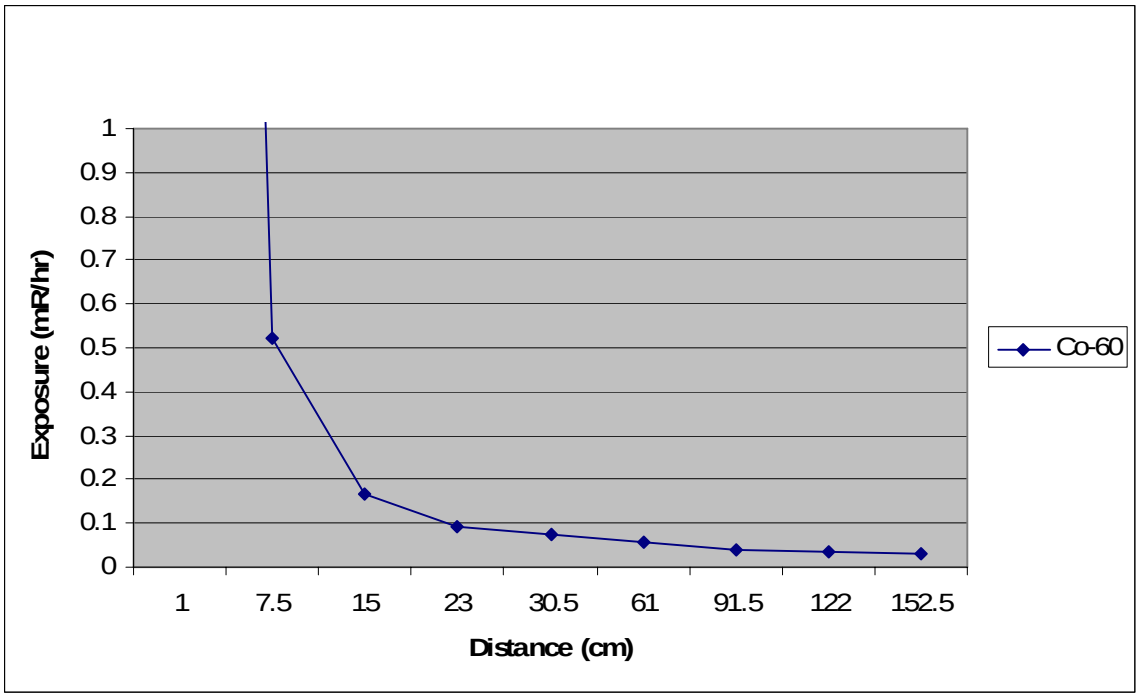

Figure 9 Exposure Rate Detected by Mini-Radiac from Co-60 Source

Comparison to the Canberra Pedestrian Portal Monitor

The Canberra pedestrian portal monitor has a nominal detection sensitivity for gamma detection of < 1 μCi for both Cs-137 and Co-60 [7]. A Mini-Radiac will never approach the detection sensitivity of such a monitor. However, in safeguard applications where the detection of sources with activity on the order of a few mCi or more is useful, the Mini-Radiac may have a role. They can be deployed in a highly distributed manner, detecting movement of sources throughout a facility. Their small size also leads to the ability to place the detectors discretely, the one sited at MURR is in a fixture that would typically house a light switch, and the final installation in fact looks like a light switch, not a radiation monitor. And of course in situations in which for whatever reason the sighting of a portal monitor is impossible, the application of Mini-Radiacs in a safeguards system can give some modicum of detection and security. This method is consistent with previous research in nuclear sensing and sensor nets.[7]

Chapter 5 Material Accounting

MATLAB Based Gamma-Ray Spectrum Simulation

A common method of passive non-destructive analysis for measuring SNM is that of gamma ray spectroscopy. This technique can be used to determine the composition of a mixed sample by analyzing the number of counts that result from the characteristic gamma ray emissions of specific isotopes. For the purposes of nuclear safeguards education, it is not often feasible to have access to the necessary equipment or materials to gain experience with using this method to measure SNM. Reference spectra exist in textbooks with the key features highlighted, but this fact merely serves to inform the student rather than to give them experience with the actual measurement method. This chapter describes the development of a script using MATLAB that can be used to simulate gamma ray spectra for a variety of radioactive samples when placed in the hands of a knowledgeable instructor. With the spectra generated by this program, students can calculate the amounts of specific isotopes in a simulated sample or simply study their characteristics.

Basics of Gamma Ray Spectroscopy

The primary isotopes that comprise uranium-based quantities of SNM are ^{235}U, ^{233}U, ^{234}U , and ^{238}U. The isotopes ^{235}U and ^{233}U are considered isotopes of SNM, whereas ^{238}U is the most naturally abundant isotope of uranium and is typically present in SNM. All of these isotopes produce gamma rays that can be used to determine their abundances in a mixed sample. In a sample of SNM, many gamma rays can be present, but certain characteristic energies with relatively high abundances stand out and can be more readily used to identify the composition of a sample. In addition, most isotopes in

SNM decay to radioactive daughters that have strong gamma ray characteristics as well [8].

Though the most interesting features of a gamma ray spectrum are the peaks that result from the characteristic gamma rays of an isotope, different mechanisms occur in gamma detection that can produce other effects in the spectrum. The primary modes of interaction that yield these effects are the photoelectric effect, Compton scattering, and electron-positron pair production. These interactions can complicate the process of determining the amount of an isotope in a sample by producing extraneous counts that cannot be easily distinguished from primary detection events. Although these effects are not desirable when taking measurements, they must be included in order to simulate a realistic gamma ray spectrum.

Each of the primary interactions cause different amounts of energy to be deposited in the detection material. In the case of the photoelectric effect, the entirety of a gamma ray's energy is deposited. Because the deposited energy is equal to that of the characteristic gamma ray, this effect results in a photo-peak that is most often used in isotope measurements. This interaction is dominant for low-energy gamma rays (less than 400 keV).

Sometimes, a gamma ray can be deflected by an electron, giving some of its energy away in the process. This phenomenon, called Compton scattering, can result in energies being deposited in the detection material that are lower than the energy of the photo-peak. As a result, a continuum of counts result that have an approximate maximum energy that corresponds to the situation in which gamma rays are scattered at 180 degrees. This maximum energy is given by equation 2 [9]:

$$E_{\gamma'} = E_{\gamma} - \frac{.511E_{\gamma}}{.511 + 2E_{\gamma}}. \quad (2)$$

However, because gamma rays can also be scattered into the detector from an external interaction, a somewhat smaller peak, called the backscatter peak, occurs at the energy given by equation 3 that mirrors the upper edge of the Compton continuum:

$$E_{\gamma'} = \frac{.511E_{\gamma}}{.511 + 2E_{\gamma}}. \quad (3)$$

These Compton scattering-related phenomena are present for all energies of incident gamma rays, but are more prominent for moderate energies (between 400 keV and 4 MeV) .

The third effect, known as pair production, is the result of a gamma ray undergoing a complete energy-to-mass conversion. The photon turns into an electron and a positron, which soon annihilates with a nearby electron, creating two 511 keV photons separated in space by 180 degrees. There are four possible outcomes of this event:

- both photons deposit their energy into the detection medium,
- one photon escapes,
- both photons escape,
- the annihilation occurs outside the detection medium, allowing one photon to deposit its energy inside the detector.

The first event will be indistinguishable from a photoelectric interaction. The second and third events will result in peaks at the primary gamma ray energy less 511 keV and 1.022 MeV, respectively. The fourth event will result in a peak at 511 keV. While these

interactions can occur for gamma rays above 1.022 MeV, they are only prominent for energies above approximately 4 MeV.

Other modes of interaction that result in small peaks are lead x-rays that result from interactions with the shielding material, and sum peaks that result from two or more photoelectric interactions that occur simultaneously (depositing a net energy of the sum of the incident energies). These interactions result in very small peaks that can be neglected for many spectroscopy applications.

When using gamma ray spectroscopy to find the specific composition of a mixed source, the resolution of the detector is very important. A low resolution detector will widen photo-peaks in the spectrum, making it difficult to discriminate individual peaks. For this reason, a high-purity germanium crystal detector (HPGe) is the most suitable detector for this type of application [10].

Experiment and Simulation

First, before any experimentation took place, an initial program was written to display a theoretical gamma ray spectrum based on gamma ray energies and their abundances that were input by the program user. This program generated spectra based on locations of photo-peaks, the Compton continuum, and pair production alone.

Ten-minute gamma ray spectra were then taken for standard sources of ^{137}Cs and ^{57}Co, and a thirty-minute spectrum was taken for a mixed standard source with ^{137}Cs, ^{60}Co, and ^{57}Co. A one-hour background spectrum was taken as well. All spectra were measured using a liquid nitrogen-cooled HPGe detector. The proprietary spectrum data was then converted to ASCII format for use with MATLAB. Two further iterations of the main program were written: One version that included the background spectrum of

the radiochemistry lab and neglected Compton scattering, and a final version that included all previous effects as well as Compton scattering and a better approximation of the photo-peaks of the gamma rays. Appendix B contains the entirety of the written program.

In order to generate accurate gamma ray spectra, several aspects of gamma ray detection needed to be considered. Primarily, the effects of the resolution and efficiency of the detector, counts in the spectrum generated by background radiation, and the three primary modes of gamma ray interaction with matter contributed to particular features of the spectrum. However, the majority of isotopes that are considered SNM do not have any characteristic gamma rays with energies that are significantly above 1.022 MeV. For this reason, the pair production phenomenon is ignored for the sake of this program, while Compton scattering and the photoelectric effect are the gamma ray interactions that are retained for analysis.

Background Radiation

The standard deviation of a measured count is approximately the square root of the count itself. Using this fact, a reasonable approximation to a realistic background count can be calculated by adding two values. The first value is the number of counts at each channel in the background spectrum. The second value is the product of a randomly generated number with a mean of zero and the standard deviation of the count (the square root of the number of counts in that channel). The RANDN function in MATLAB produces a random normal number with a standard deviation of one. Using the expression in equation 4 at each channel number produces an appropriate background spectrum:

$$newcounts = \sqrt{counts} \times randn + counts. \quad (4)$$

Figure 10 shows the measured 60-minute background spectrum and a randomized version of this same spectrum. The primary features of interest are peaks at channel 729, which corresponds to the 1460 keV gamma ray from the ^{40}K that is present in the walls of the laboratory, and channels 331 and 61, which correspond to the 662 keV and 122 keV gamma rays from the large amounts of ^{137}Cs and ^{57}Co, respectively that are present in the room. The low-energy rise of the spectrum is largely due to a combination of Compton effects from higher-energy gamma rays and various electronic noise.

Photo-Peaks

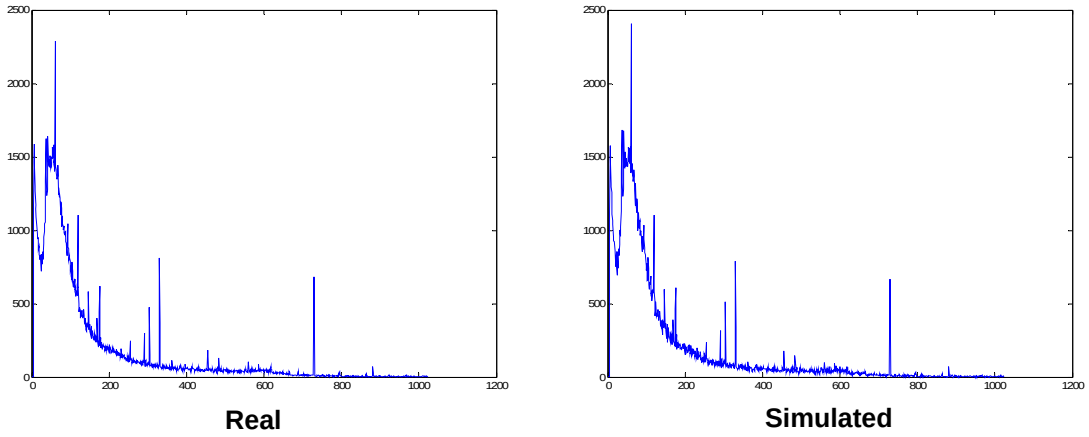

Figure 10 Real and Simulated Background Spectra

Photo-peaks in a gamma ray spectrum measured by a HPGe detector are not infinitely narrow spikes that lie at the energy of the gamma ray. In reality, while the high resolution of germanium-based detectors allows for easy determination of peaks in close proximity, imperfections in the detection system cause a slight widening of the photo-peaks. From experimentation, the spectrum drops to a value very close to background for

energies higher than that of the gamma ray. However, for energies lower than the photo-peak energy, a slightly slower drop-off occurs that resembles a steep exponential curve.

A reasonable approximation to the shape of this photo-peak is the histogram of a random normal number that is forced to be negative. After much trial-and-error, the best approximation occurs with a histogram of the expression in equation 5, where RANDN(N,1) generates N random numbers. In practice, the best quality approximation is given when N is equal to the number of counts in the photo-peak, which is a logical choice. Figure 11 shows a comparison of a histogram generated using this method and the experimentally measured photo-peak of ^{137}Cs.

$$values = -\frac{1}{2}\left|randn(N,1)\right|^3 \tag{5}$$

It is not possible to superimpose this histogram onto the background spectrum in the simulation. In order to incorporate this approximation, it is necessary for the program to add the number of "counts" that fall within an energy region and add this number to the energy spectrum at the appropriate channel. An efficient method to implement this concept is to round the values generated for the histogram to integer values (this is acceptable because the spectrum is only defined for discrete channel numbers) and increment the spectrum at each energy channel by the number of times that channel appears.

Detector Efficiency

This approximation of a photo-peak works well because the number of counts that are randomized into a photo-peak is equal to the number of counts registered by the detector experimentally. However, the number of counts registered by the detector is often much lower than the number of atoms of the sample that will decay during the

measurement [10]. To calculate the number of counts that will exist in a measured photo-peak from the activity of the sample, the efficiency of the detector must be known.

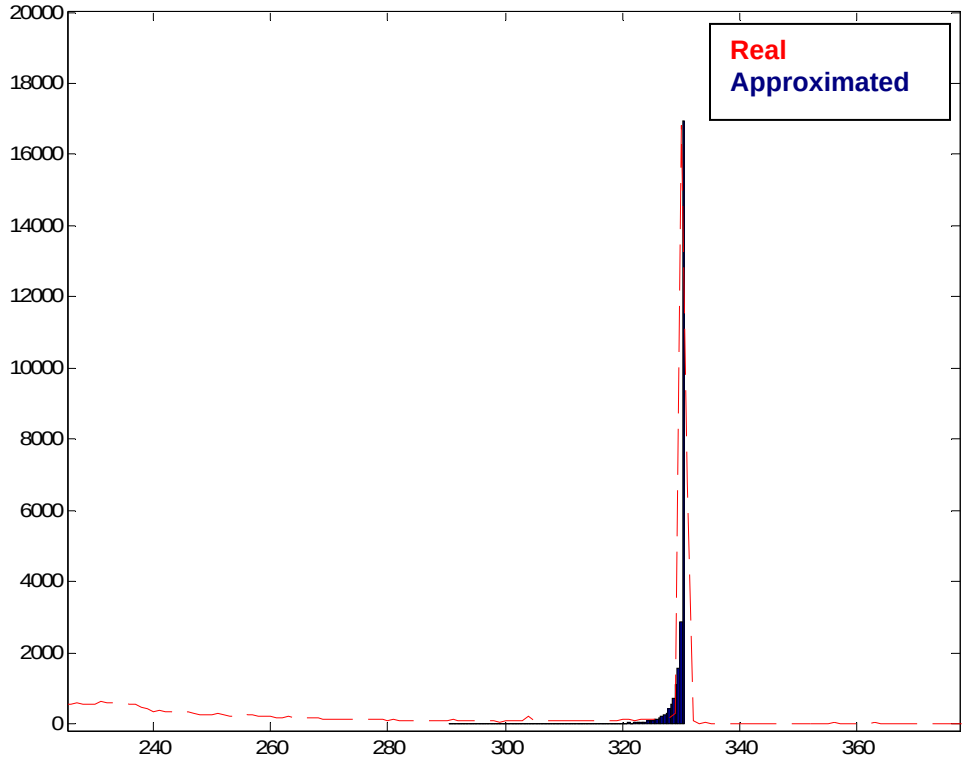

Figure 11 Comparison of Real and Approximated Photo-Peaks

Two aspects of detection affect the overall efficiency: the proportion of gamma rays that do not interact with the detection material, called the intrinsic efficiency, and the proportion of gamma rays that simply do not pass through the detection material, called the geometric efficiency. The geometric efficiency only depends on the physical layout of the detection system, and as such, can be input by the program user. The intrinsic efficiency, however, depends on the energy of the gamma ray, and is best determined experimentally. By measuring a mixed sample with a variety of gamma ray energies and a known activity, the resulting spectrum can be used to generate a curve that can be used

to estimate the intrinsic efficiency of the detector for varying gamma ray energies [10]. The standard used for this efficiency calibration includes ^{57}Co, ^{137}Cs, and ^{60}Co, giving four primary gamma ray energies. By performing a linear fit on a logarithmic plot of the efficiencies at these energies as shown in Figure 12, it was found that the expression given by equation 6 gives a good approximation to the efficiency of the detector at the gamma ray energy E:

$$\mathrm{eff}(E) = e^{-1.1\ln(E)+2.8}. \tag{6}$$

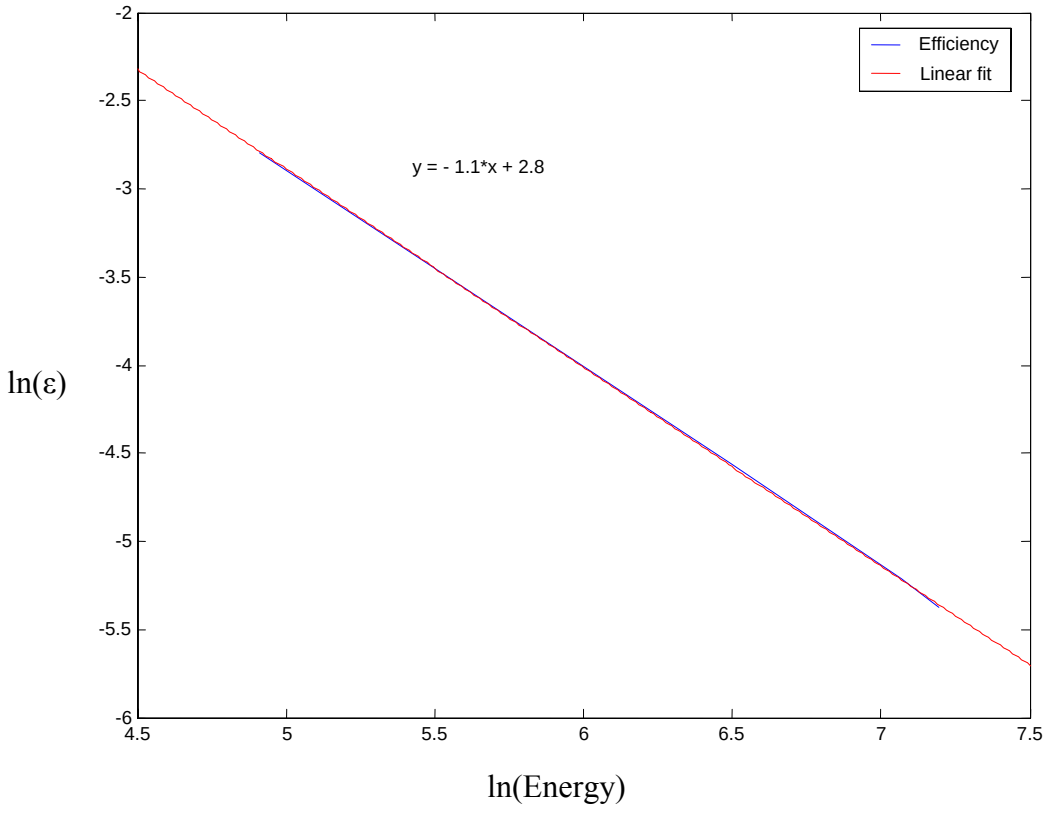

Figure 12 Efficiency Curve for Gamma Ray Spectrum of Measured Standard.

Compton Scattering

Due to the nature of Compton scattering, the Compton edge, continuum, and backscatter peaks are the most difficult aspects of the spectrum to simulate. The location of the Compton edge and the backscatter peak can be calculated as long as the gamma ray energy is given, but the exact shape and size of the continuum can vary substantially based on the gamma ray energy and the size of the detector [9, 10]. The most practical solution in this case is to isolate the Compton continuum from the measured spectrum of a standard with a single gamma ray and manipulate this continuum to apply to other situations. Given the sources available, a ^{137}Cs standard seems to be the most suitable isotope as it emits a single gamma ray of a medium-range energy. By subtracting the measured background spectrum from the measured ^{137}Cs spectrum, the region below the energy of the photo-peak can be considered to be a reasonable approximation to the actual Compton continuum. Because the basic shape of the continuum only changes a small amount for differing gamma ray energies, this approach only requires the height and width of the continuum. One way to determine the width of the Compton continuum is to find the energy of the Compton edge using equation 1. Assuming a linear relationship between the location of the Compton edge and the locations of the features in the continuum—which is not strictly accurate but serves well in this application—the ^{137}Cs continuum can be expanded or compressed accordingly to the energy of the gamma ray in question. Using the INTERP1 command in MATLAB, a one-dimensional array of data can be interpolated from one set of independent axis values to another. This step is very important; if a data set is shifted from a narrow to a wide set of channels without interpolation, many values indexed to the new set of channels will be assigned zero

counts. Figure 13 shows a comparison between the original Compton continuum taken from ^{137}Cs and a version of this continuum stretched to three times its original width. It can be seen from this graph that the primary features of the continuum are preserved with expansion. The most obvious deficiency to this approach is the fact that the measured backscatter peak moves relative to the Compton edge as well. Fortunately, the height of the backscatter peak relative to that of the rest of the continuum is small, and is not easily distinguishable when displayed using a logarithmic plot.

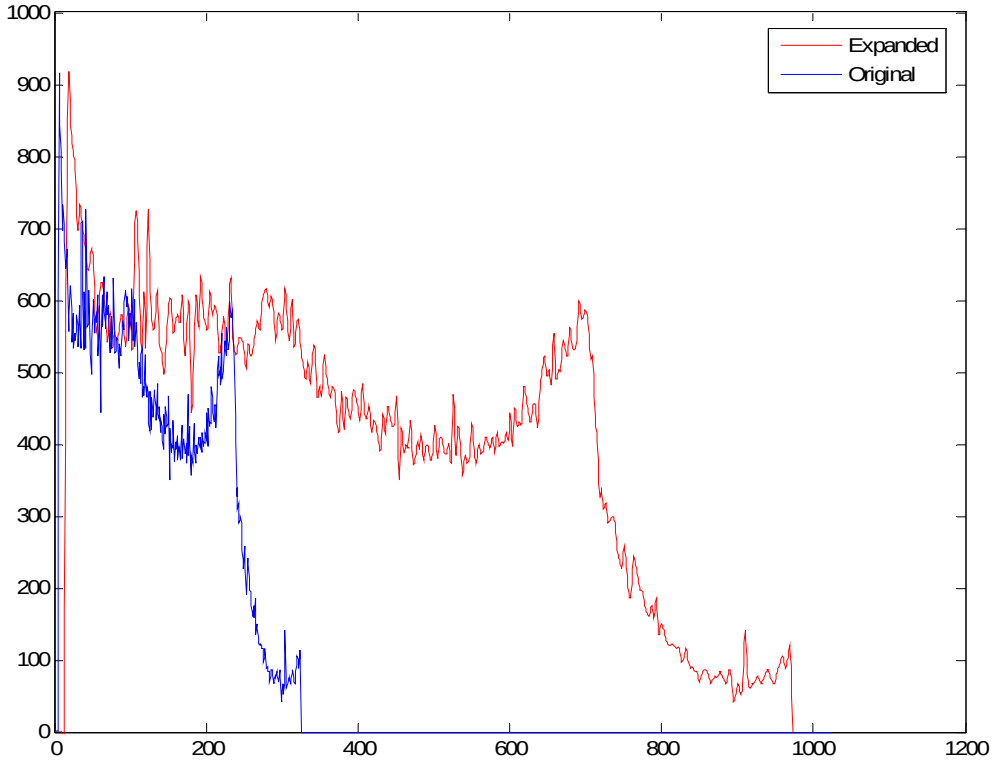

Figure 13 Interpolated Compton Continua.

However, because the height of the continuum relative to that of the photo-peak also varies with the energy of the incident gamma ray, it is necessary to determine a relationship that can be used to determine the height based upon energy. After experimenting with different methods, the most useful relationship is a graph of the ratio between the height of a photo-peak and that of its associated Compton edge. However,

when analyzing the spectrum measured for the mixed standard used in finding the efficiency curve, it is important to note that Compton continua for multiple photo-peaks will interfere. For this reason, it is necessary to subtract the Compton background from the counts at each Compton edge to achieve the most accurate estimate of its height. Figure 14 shows a plot of the ratio of Compton edge counts to photo-peak counts vs. incident gamma ray energy. A linear fit of this plot estimates that this ratio can be estimated as a function of energy using equation 7:

$$ratio = 4.4 \times 10^{-5}(E_\gamma) + .011. \tag{7}$$

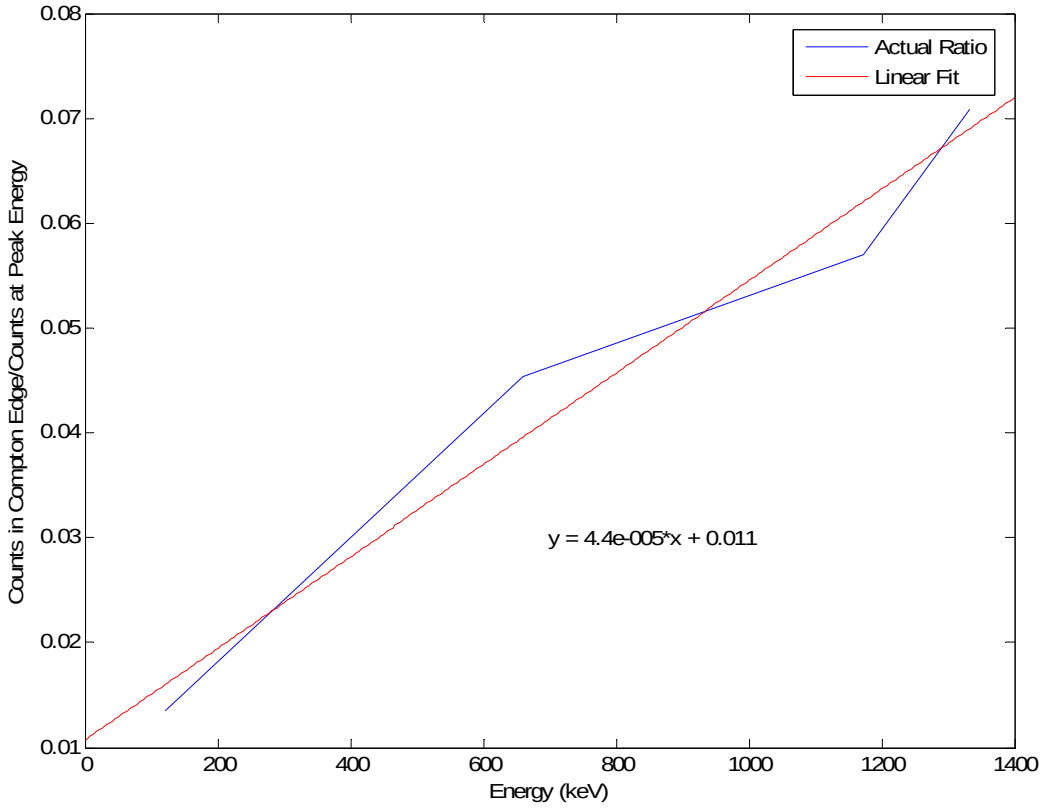

Figure 14 Linear Fit of the Relative Heights of Compton Edges for Varying Energies.

Mixed Samples of SNM

As written, this script uses gamma ray energies and abundances supplied for a single isotope to generate a simulated spectrum. For samples with only a single radio-

isotope, this is sufficient. However, to simulate the spectrum for a sample with a mixture of radio-isotopes, this method is not sufficient. Two main solutions were considered: either the inclusion of code that prompts the user for multiple isotopes to be included as well as their isotopic abundances and adjusts the gamma ray abundances accordingly, or treating a mixed sample as a single isotopic source and calculating adjusted gamma ray abundances before supplying the data. Due to time and programming constraints, the latter approach was chosen. For a mixed sample with multiple radioactive isotopes, the abundances of gamma rays are different than for those of a single isotope. However, not only the isotopic abundances, but the differences in decay constants need to be considered in order to compute modified abundances. For instance, if a sample were to contain 5% ^{234}U and 95% ^{238}U, the majority of decay events would be the result of ^{234}U rather than ^{238}U decay as the decay constant of ^{234}U is approximately 2000 times as large as that of ^{238}U. In order to compute these adjusted abundances, it is necessary to know the average atomic weight of the mixed sample as well as its decay constant. Using equations 8 and 9, these values can be found, and equation 10 can be used to find the percentage of decay events that will result from isotope N in a sample.

$$A_{sample} = \sum_{N} IR_N A_N \tag{8}$$

$$\lambda_{sample} = \sum_{N} IR_N \frac{A_{sample}}{A_N} \lambda_N \tag{9}$$

$$\%Decay_N = \frac{\lambda_N IR_N \left(A_{sample} / A_N \right)}{\lambda_{sample}}. \tag{10}$$

The term IR_N is the isotopic ratio of the isotope N, A_N is the atomic weight of isotope or sample N, and $\%Decay_N$ is the percentage of decays in the mixed sample that result from

isotope N. These equations are based on derivations from the fact that the percent of decays in a mixed sample that result from isotope N is equal to the activity of isotope N divided by the total activity of the mixed sample. Multiplying $\%Decay_N$ by the natural abundance of a gamma ray gives its true abundance in the mixed sample in question. Table 5 gives $\%Decay_N$ values for four common mixed uranium materials: Natural uranium, low-enriched uranium (enriched to 5% ^{235}U), highly-enriched uranium (enriched to 20% ^{235}U), and weapons-grade uranium (enriched to 85% ^{235}U). Using these values to modified standard gamma ray abundances, data can be entered for each sample to be used by the script as if the sample consisted of a single radio-isotope.

Table 5 Percent-decay Values for Mixed Uranium Samples.

Sample	$\%Decay_{234}$	$\%Decay_{235}$	$\%Decay_{238}$
Natural U (.72% ^{235}U, 99.275% ^{238}U)	50.84%	2.19%	47.00%
LEU (5% ^{235}U)		25.28%	74.72%
HEU (20% ^{235}U)		61.65%	38.35%
Weapons-grade (85% ^{235}U)		97.32%	2.67%

Results/Discussion

Figures 15 through 18 show simulated spectra for natural uranium, LEU, HEU, and weapons-grade uranium, including all gamma rays that are at least .01% naturally abundant. This limitation is necessary because the photo-peak approximation becomes weak for low numbers of counts. The isotope ^{235}U has 42 specific gamma rays included in this simulation, whereas ^{238}U and ^{234}U only have two each. The most prominent gamma ray of ^{235}U is the 57.2% abundant 185.712 keV gamma ray, which appears on channel 93 of the spectrum. Comparing relative heights of this gamma ray among the different graphs shows what one would expect: for increasing isotopic abundances of ^{235}U, the 185.712 peak (as well as the other characteristic peaks of ^{235}U) increases in

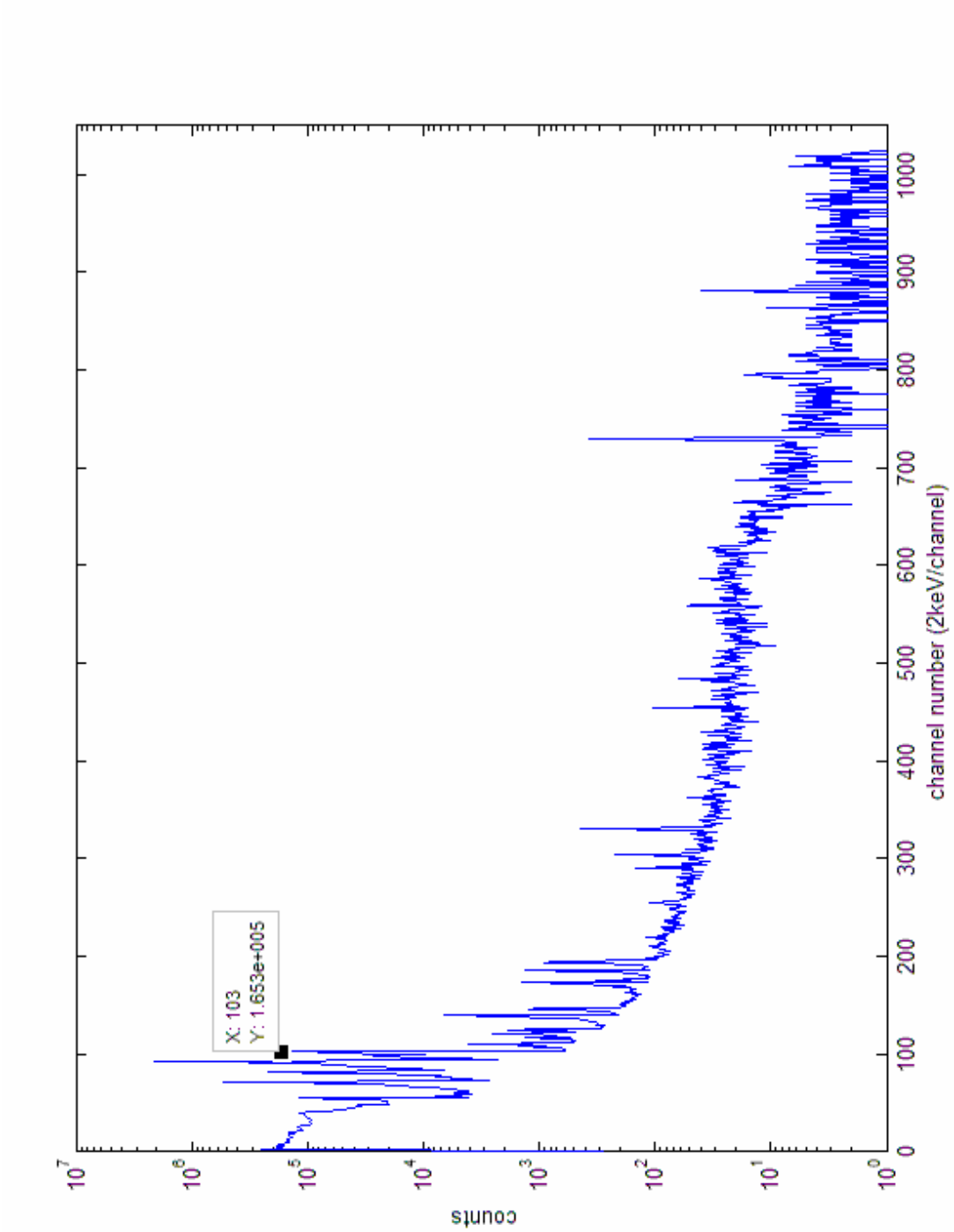

Figure 15 Gamma Ray Spectrum for Highly-Enriched Uranium

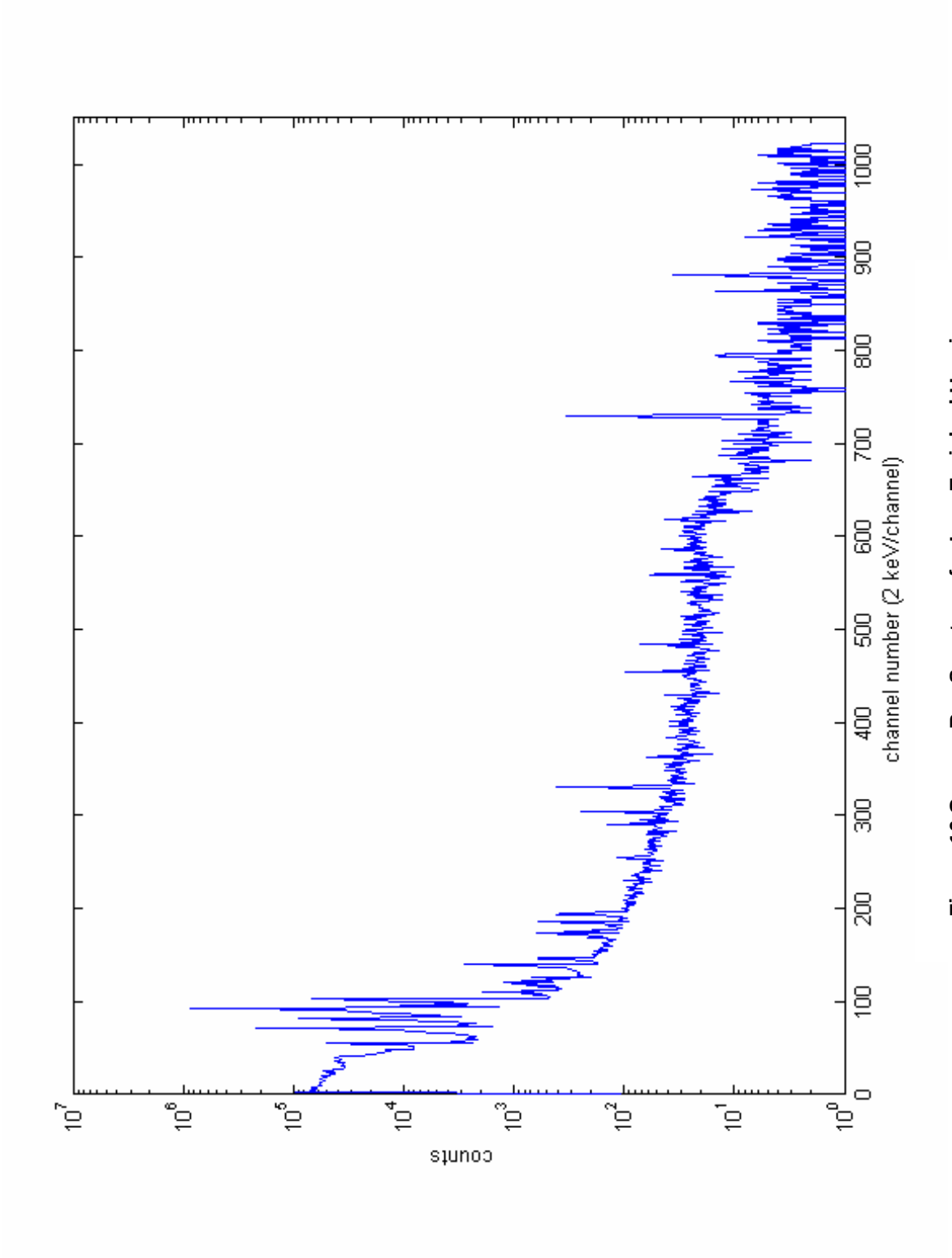

Figure 16 Gamma Ray Spectrum for Low-Enriched Uranium

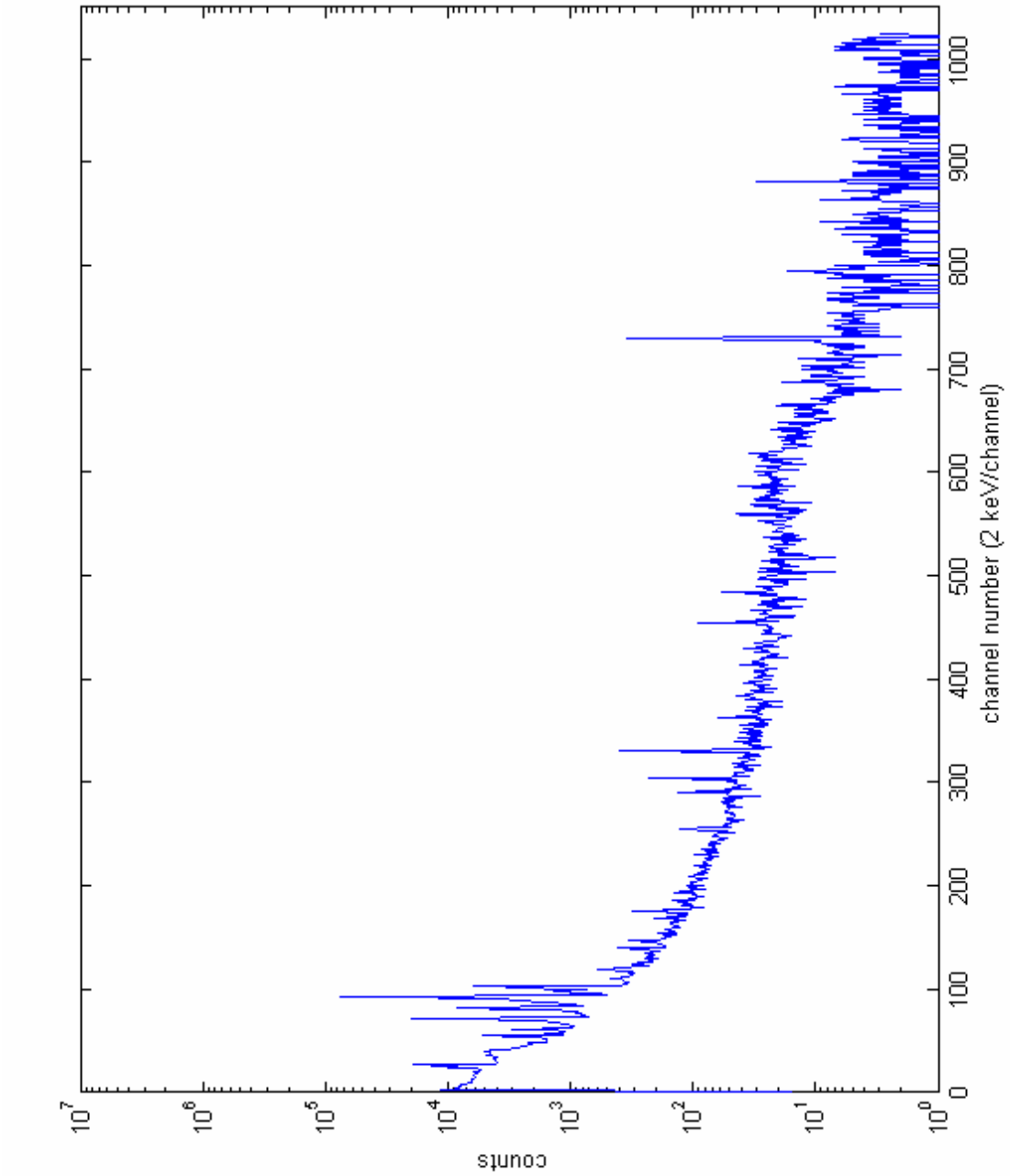

Figure 17 Gamma Ray Spectrum for Natural Uranium

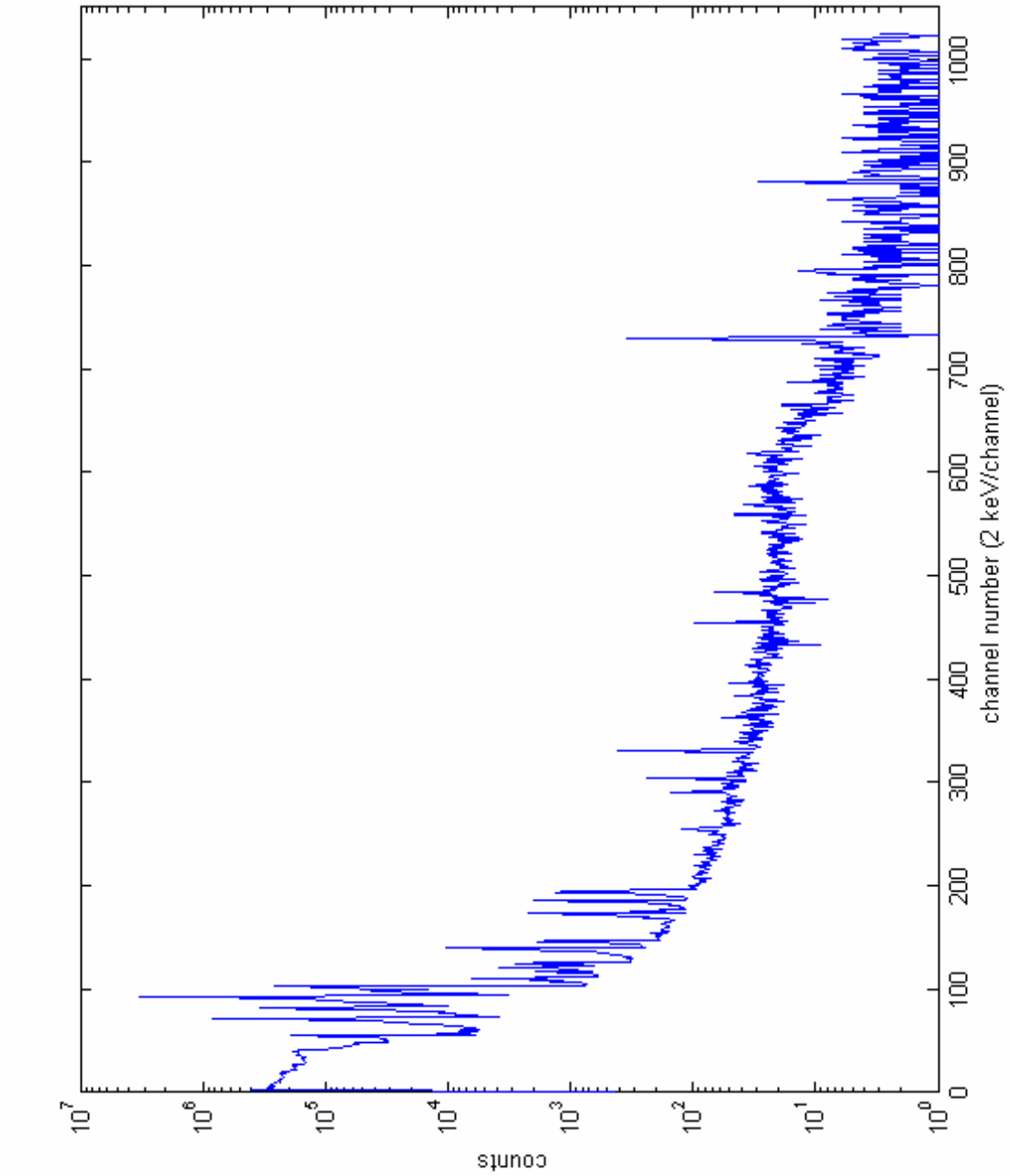

Figure 18 Gamma Ray Spectrum for Weapons-Grade Uranium

height. All of these simulations were performed using 5 μCi sources for thirty-minute count times and a geometric efficiency of 50%.

These spectra have a few deficiencies and specific considerations. Many of these deficiencies arise from the way in which the Compton continuum was generated. First, the backscatter peaks are included in the continua that are generated for each photo-peak, and are not located at the correct energy channels. However, as stated previously, the backscatter peak from the sampled continuum is small and is nearly indistinguishable in a logarithmic plot. Additionally, simulated backscatter peaks have been excluded from the plot. From the low abundance of the majority of gamma rays as well as the low energy of the most abundant gamma rays, this appears to be a reasonable omission. Finally, the method used to interpolate the original continuum to varying widths has inherent problems, as the relationship between the Compton edge and the remainder of the counts in the complete continuum is not linear, but is assumed so for this application. As a result, for gamma rays with energies lower than 662 keV (which corresponds to the example spectrum of ^{137}Cs), the region between the Compton edge and the photo-peak contains errors, as there exists a gap for which the interpolated continuum is not defined. Sum peaks have also been ignored, as the amount of code and processing power required to cross-reference all characteristic gamma rays with one another and produce appropriate peaks would not be worth the effect that would be observed in the spectrum. In addition, sum peaks did not appear to be prominent features of the experimentally measured spectra. Finally, these peaks assume that the samples for which spectra are simulated have been measured in the room in which the experimental spectra were taken.

In a more realistic setting, such as a weapons facility or a uranium milling plant, the background spectrum could potentially be much different.

The gamma ray spectra simulated by this script provide a good approximation to experimentally measured spectra. These generated data can be used to provide practical experience to students in the analysis of actual spectra without the expense or complication in using detection equipment and quantities of SNM to produce experimental data. By comparing the gamma ray peaks in the generated spectra, a student should be able to determine the approximate enrichment of a given theoretical sample.

Chapter 6 Conclusion

While the task of developing applied coursework in the field of nuclear safeguards is certainly difficult, simulations and experiments such as those presented here can aid in giving students and safeguards workers practical experience. The experiments demonstrated here present an introduction to general nuclear safeguards principles that can be expanded upon in the future to help establish a complete nuclear safeguards education. Each section in material protection, control, and accounting was undertaken to satisfy contemporary needs in the education of nuclear safeguards.

The other classes required for the nuclear safeguards certificate that were offered prior to the introduction of the nuclear safeguards course are instrumental to a full understanding of nuclear safeguards in general. Radiation Safety and Radiation Detection cover the fundamentals of practical nuclear science and technology, while Nonproliferation Issues involves cultural, political, and other contemporary considerations necessary to understand the safeguards philosophy. Finally, The Nuclear Safeguards Science and Technology course brings these concepts together to form a coherent vision of the protection, control, and accounting of nuclear material.

In the future, advances could be made that would allow for a complete educational experience in nuclear safeguards. Beginning with a fictitious quantity of SNM to be detected, a complete system of accounting, shipping, intra-facility control, and physical protection could be designed and implemented from the basics introduced and considered here. The only aspect of nuclear safeguards education that strictly requires radioactive material is measurements as part of material accounting. As shown

here, it is possible to simulate these measurements in order to impart practical experience to a student.

REFERENCES

1. M.L. Garcia, *The Design and Evaluation of Physical Protection Systems*, Elsevier Science, Burlington, Ma, 2001.
2. J.R. Rodriguez, B. Dry and J.C. Matter, "Intrusion Detection Systems," Sandia National Labs, SAND91-0948, 2001.
3. D.R. Joy, *An Introduction to the Nuclear Fuel Cycle and Nuclear Safeguards*, JAI Corporation, Fairfax, Va, 1999.
4. J. Ball et al., "Sensitivity Analysis of Adversary Interruption at Typical Research Reactor Sites Utilizing EASI", 47th INMM Conference, Nashville, Tn, 2006.
5. J. Gahl, et al., "The University of Missouri Research: Operations Monitoring Test Site and Safeguards Training Facility," Proc. of the Institute of Nuclear Materials Management, 2004, Orlando, FL, USA.
6. J. Neustrom, et al., "Enhancement of the Nuclear Safeguards Demonstration System at the University of Missouri Research Reactor," Proc. of the Institute of Nuclear Materials Management, 2005, Phoenix, USA.
7. Canberra-Aquila Inc., "CPM-PGN Pedestrian-Gamma/Neutron Monitor," http://www.canberra.com/products/1190.asp, October 2003, USA, last views June 15, 2006.
8. D. Reilly, N. Ensslin, H. Smith Jr., S. Kreiner, "Passive Nondestructive Assay of Nuclear Materials," Los Alamos National Laboratory, NUREG/CR-5550, Washington DC, March 1991.
9. D. Ehmann, D.E. Vance, *Radiochemistry and Nuclear Methods of Analysis*, John Wiley Sons, Inc., New York, NY, 1991.
10. W. Wang, C.H. Willis, D. Loveland, *Radiotracer Methodology in the Biological, Environmental, and Physical Sciences,* 1975
11. A.V. Korolev, A.N. Rumyantsev, "'Probabalistic Expert-Advisory System' Program Package for Probabalistic Analysis of Complex Technical Systems," Atomic Energy, vol. 90, no 2, p.95, 2001.
12. S.E. Jordan et al., "Discrete-Event Simulation for the Design and Evaluation of Physical Protection Systems," 1998 Winter Simulation Conference Proceedings, vol.1, p. 899 Piscataway, NJ, USA, 1998.
13. C. Kim, S. Kwak, C.H. Chung, "A Simulation Methodology for the Evaluation of the Physical Protection Systems in Nuclear Power Plants," *Transactions of the American Nuclear Society*, vol.93, p. 320, 2005.
14. W.C. Priedhorsky, "Physical and Economic Limitations for Distributed Nuclear Sensing," Journal of Nuclear Materials Management, Vol. 34, No. 3, Spring 2006, Los Alamos, NM, USA.
15. P.A. Korstad, "Accounting Systems for Special Nuclear Material Control," Battelle-Pacific Northwest National Laboratory, NUREG/CR-1283,Washington DC, January 1980.
16. D.R. Rogers, "Handbook of Nuclear Safeguards Measurement Methods," Monsanto Research Corporation, NUREG/CR-2078, Washington DC, September 1983.

Appendix A Sample EASI Spreadsheet

	A	B	C	D	E	F	G
1							
2			***Estimate of Adversary Sequence Interruption***	Probability of Guard Communication		Response Force Time (in Seconds) Mean	Standard Deviation
3				0.95		300	90
4							
5							
6							
7							
8							
9							
10							
11							
12							
13							
14							
15							
16							
17							
18							
19							
20							
21							
22							
23							

Task	Description	P(Detection)	Location	Delays (in Seconds): Mean:	Standard Deviation
1	Cut Fence	0	B	10	3
2	Run to Building	0	B	12	3.6
3	Open Door	0.9	B	90	27
4	Run to Vital Area	0	B	10	3
5	Open Door	0.9	B	90	27
6	Sabotage Target	0	B	120	36
7					
8					
9					
10					
11					
12					

Probability of Interruption:	0.476040779

Appendix B Code for Spectrum Generation Script (with comments)

CODE FOR GENERATING SPECTRA

```
% Phase 1 of the spectrum generating program; Theoretical spectra are
% calculated and displayed based on user-input about the detector and the
% sample to be counted.  The resolution of the detector and other random
% processes are not accounted for.  Placeholders are used for the intrinsic
% efficiency of the detector at each energy (10% for now) and to determine
% the relative heights of various peaks.  Ideally these factors will be
% approximately determined through experimentation.  Later, I plan to
% adjust the user input so that instead of inputting individual gamma
% energies, the user can supply the isotopes and amounts by weight
% abundance in the sample, and the software will index the energies on its
% own.

%Phase 2 changes:  Now, instead of specifying the gamma data, the user is
%asked to choose an isotope whose gamma data will be used.  The list of
%isotopes are generated from isotopelist.txt which is generated by
%isotoperegistry.m.  Gamma data is gathered from files that are generated
%invdividually by isotoperegistry.m.  At this point, only a single isotope
%can be used at a time.  In a future iteration, I'd like to improve on this
%such that a mixture of isotopes can be specified using either weight
%percentages or activities of each portion of the whole.
%Coming soon regarding spectrum generation:  Normal random generation of
%each peak for each count based on the parameters of peaks found in real
%gamma spectrum counting.

%Phase 3 changes:  Background is now taken from background.txt (this is an
%experimental 1 hour background count).  This background is divided by 3600
%(the original count time) and then multiplied by the count time in
%seconds.  This background is added to the total spectrum.  The photopeaks
%are now simulated by a cubed random normal number generator that is
%centered around the peak energy and made to be negative (to the left of
%the peak).  The efficiencies are now taken from an experimentally-determined log-log
%curve over the range of 2.048 MeV energies.  Finally, the Compton
%continuum for each photopeak is taken from the experimentally measured
%continuum of Cs-137 and expanded or compressed and resized to fit the
%needs of the photopeak in question.


countsec = input('Counting time in seconds:');
Spectrum = ones(1024,1);
bgspec=zeros(1024,1);
```

```
fid=fopen('background.txt','r');   %reads experimental background data from file
bgspec=fscanf(fid,'%f\n');
fclose(fid);

fid=fopen('compton.txt','r');   %reads experimental compton data from file based on cs
spectrum
ccspec=fscanf(fid,'%f\n');
fclose(fid);

ccspec=ccspec/(600*6*1.41);

bgrate = bgspec/3600;

N=1;                %randomizes background; uncertainty at each energy is the square root
of the counts at that energy
for N=1:1024;       %1024 samples, but channel-to-energy conversion is 2keV per channel.
Spectrum(N,1)=(sqrt(bgspec(N))/3600*randn+bgrate(N))*countsec;   %randn generates
random normal numbers with a mean of zero and a standard deviation of 1
Spectrum(N,1)=round(Spectrum(N,1));         %ensures counts are integers
if Spectrum(N,1)<0;   %ensures counts are positive
Spectrum(N,1)=1;
end
end

Spectrum(1)=Spectrum(2);  %set counts at 1keV equal to counts at 2keV to make
programming easier

Energies = 1:1:2048;
Eff = exp(-1.1*log(Energies)+2.8);            %Spectrum of experimentally-measured
efficiencies

fid=fopen('isotopelist.txt','r');             % Open list of registered isotopes and read list of
names with the following lines.

C=fgetl(fid);

while feof(fid)==0
   C=strvcat(C,fgetl(fid));
end

fclose(fid);
for(a=1:size(C,1))            %Here a list of numbered isotopes is given for the user to
choose from.
   disp(strcat(int2str(a),'-',C(a,:)));
end
```

```
IsoInd=input('Which isotope would you like to use? ');   %User enters number for the
desired isotope.

Isotope = C(IsoInd,:);

filename=strcat(Isotope,'.txt');  %Filename is constructed for the desired isotope

fid=fopen(filename,'r');   %File for the isotope is opened and the gamma data read with
the following lines.
E=fscanf(fid,'%f %f\n',[2,inf]);
E=E';

fclose(fid);

Act = input('Activity of sample (mCi) = ');   % Prompt for activity
Z = 32;  % Z is given for germanium crystal detectors
Act = Act*3.7E7;                          %  Convert activity to dis/second
N = size(E,1);      %Number of gammas = number of rows of E
GEff = input('Geometric Efficiency of the Detector (percent) = ');
GEff = GEff/100;


a=1;
while a<N+1
E(a,1) = round(E(a,1)/2);               % Fix gamma energy to an integer value for indexing,
2keV/channel conversion
E(a,2) = E(a,2)/100;                  % Convert from percent to ratio

%Photopeaks

Photopeaks = Act*E(a,2)*Eff(2*E(a,1))*GEff*countsec;   %Calculates number of counts
that should appear in the photopeak

photospread=-abs(.5*abs(randn(round(Photopeaks),1)).^3)+ E(a,1);
photospread=round(photospread);
for M=max(photospread):-1:1
        Spectrum(M)=Spectrum(M)+length(find(photospread==M));
end

%Compton Effect

b=(2*E(a,1)-(1000*.511*2*E(a,1)/1000)/(.511+2*(2*E(a,1)/1000)))/462;   %finds ratio
of new compton edge to reference compton edge from cs137

peak = Spectrum(E(a,1));    %tells me how many counts exist at the peak energy
```

```
c=4.4E-5*2*E(a,1)+.011;     %determines the relationship between the number of counts at the peak energy and the height of the compton edge
cemag = c*peak;             %normalize to 1  (reference compton edge has magnitude of ~600)

newcomp = countsec*cemag*interp1(1:325,ccspec(1:325),1:1/b:325,'v5cubic');
%interpolates missing data (also crunches data if b<1) to the proper width of the continuum.

for d=1:length(newcomp)
   Spectrum(d)=Spectrum(d)+newcomp(d)*(d<E(a,1));   %adds compton continuum to the current spectrum.
end


a=a+1;    %Ready for the next gamma
end

for N=1:1024     %gets rid of negative or zero counts for the sake of making the log-plot easier
   if Spectrum(N)<1
      Spectrum(N)=1;
   end
end

semilogy(round(Spectrum));   %Rounds to integer values of counts and displays on a semi-logarithmic plot.
```

CODE FOR REGISTERING ISOTOPES FOR USE IN SPECTRA

```
filename = input('What isotope would you like to enter? (no spaces, please!)  ', 's');

N = input('Number of Gammas = ');
E = zeros(N,2);                          % Declare matrix of energies and their abundances

a=1;

while a<N+1
E(a,1) = input('Gamma ray energy (keV) = ');    % Prompt user for gamma ray energies and abundances
E(a,1) = round(E(a,1));                  % Fix gamma energy to an integer value for indexing
E(a,2) = input('Abundance of Gamma (percent) = ');
E(a,2) = E(a,2);
```

```
a=a+1;
end

fid=fopen('isotopelist.txt','r');  % Open file to read already-existing isotope list

C=fgetl(fid);    %Obtain list

while feof(fid)==0
   C=strvcat(C,fgetl(fid));   %Add new isotope to list
end

C=strvcat(C,filename);

fclose(fid);

fid=fopen('isotopelist.txt','w');   %Open isotope list for writing

b=1;

for(b=1:size(C,1));   % Write updated list to the file
fprintf(fid,'%s',C(b,:));
fprintf(fid,'\n');
end

fclose(fid);


fid=fopen(strcat(filename,'.txt'),'w');   % Create new file from the name of the isotope and
write gamma data to file
fprintf(fid,'%f %f\n',E');
fclose(fid);
```